Chapter 1

Quantum integrated photonic circuits

Samir Bounouar*, Marcelo Davanco†, and Stephan Reitzenstein*,1
*Technische Universität Berlin, Institute of Solid State Physics, Hardenbergstrße 36, D-10623 Berlin, Germany , †National Institute of Standards and Technology, Gaithersburg, Maryland 20899, United States

ABSTRACT
Integrated quantum nanophotonics aims at combining optical elements on-chip to realize complex circuits with full quantum functionality. Examples are integrated boson sampling circuits and chips that generate 2D photonic cluster states. As such, this modern field of photonics opens up many exciting opportunities in quantum technology with the overarching goal of implementing large quantum networks and photonic quantum computers. This chapter provides an overview of important basics of integrated quantum nanophotonics, represents the state of the art and provides an outlook on possible future developments. It includes an insight into numerical design and optimization processes and introduces modern manufacturing processes for quantum circuits. Based on this, corresponding circuits relying on homogeneous semiconductor structures are discussed, with a focus on elements with integrated quantum emitters. In addition, advanced concepts are also presented, which are enabled by the heterogeneous combination of different materials in order to develop fully integrated quantum chips. The chapter closes with an outlook on future developments and a summary.

KEYWORDS
Integrated quantum nanophotonics, Quantum technology, Quantum emitter, Quantum dot, Waveguide, Single-photon emitter, Single-photon detector

1.1 INTRODUCTION

Integrated quantum photonic circuits (IQPCs) are key elements in the emerging field of quantum technologies. They provide exciting opportunities to realize quantum devices with high functionality in a scalable, robust, energy efficiency and compact fashion. Similar to the development in of integrated electronic circuits in the 1960s, it is expected that IQPCs will boost the progress in the field and lead to high-performance quantum systems to perform, for instance, quantum computation and quantum simulations [78, 44]. Here, scaling up to quantum

1. Email: stephan.reitzenstein@physik.tu-berlin.de

operations with $N \gtrsim 50$ qubits promises to outperform classical computers and to enter the regime of quantum supremacy [99, 6]. The overarching motivation for the development of IQPCs is based on the efforts to reduce complex and sensitive laboratory structures to a chip level. As with electronically integrated circuits, this leads to a significantly increased functional density and is the basis for successfully transferring exciting basic experiments into real applications of quantum technology with low operation costs.

Depending on the intended task, IQPCs have different levels of complexity, but they have in common that the relevant information is transmitted within the circuits by means of individual photons. In the simplest case, they only contain photonic waveguide (WG) structures, beam splitters and possibly phase shifters to perform basic quantum operations [78, 128]. However, much more complex architectures are required for many goals and advanced applications, such as the generation of 2D photonic cluster states, multidimensional quantum entanglement and the realization photonic quantum computers [12, 136, 113, 55, 191]. In addition to simple WG structures, fully integrated IQPCs ideally also include active elements such as single-photon emitters, which in the best case are also excited directly on the chip electrically via carrier injection or optically via integrated micro- or nanolasers. Such circuits quickly become more complex and require sophisticated design concepts and manufacturing processes. In addition, the combination of several material systems in heterogeneous approaches is often required in order to be able to map all the necessary functionalities. For example, it makes sense to combine quantum dots (QDs) in the GaAs material system in hybrid architectures with loss-minimized silicon waveguides in order to, respectively, generate single photons at high rate and to transfer and manipulate them in the silicon waveguides with low optical losses [200, 76, 23, 155]. Similarly, it is attractive to combine superconducting materials with waveguide materials to implement on-chip single-photon detectors [120, 137] and recently even fully integrated Hanbury Brown and Twiss experiment [161].

The development of IQPCs promises exciting opportunities across the board to implement components with high quantum functionality. In addition to the underlying ideas and sophisticated numerical design methods, advanced manufacturing methods must be developed and applied. In some cases, methods of classic integrated photonics can be used to implement low-loss silicon WGs, for example. For the envisioned operation in the quantum regime of individual emitters and individual photons, however, new types of technology concepts have to be established. For example, the targeted and scalable integration of individual quantum emitters in IQPCs represents a major challenge that can only be solved with new approaches in the field of quantum technology and quantum engineering. In this context, deterministic manufacturing processes have been developed in recent years to select individual quantum emitters based on their optical properties and to integrate them into WGs with nanometer accuracy. In addition, methods for spectral control of individual quantum emitters have been established that form the basis for IQPCs whose functionality is based on

multiphoton interference, when implementing, for instance, large scale boson sampling circuits or scalable quantum computing using the Knill-Laflamme-Milburn (KLM) scheme [78, 182]. In addition, it has been proposed to implement IQPCs using quantum physical effects such as entanglement to generate 2D photonic cluster states as key resource for universal measurement-based quantum computation [185]. These concepts and many other approaches in the field of photonic quantum technology benefit decisively from the integration of optical components in functional IQPCs, which explains the high interest and the timely importance of developing such elements.

Against this background, this chapter shows important basics and current developments in the field of IQPCs. The aim is to give undergraduate students, doctoral students and interested scientists from related subject areas a well-founded insight into the topic and also to show the enormous potential and future developments of integrated quantum nanophotonics. Following the thematic introduction in the present section, section 1.2 introduces numerical methods that are used for the design and functional optimization of corresponding quantum optical circuits. Building on this, section 1.3 gives an insight into modern manufacturing methods for IQPCs. One focus here is on novel and unconventional approaches that have been developed to integrate quantum emitters in a highly controlled manner as single photon sources in quantum circuits. Sections 1.4 and 1.5 include an overview of the current status in the development of quantum circuits based on homogeneous material compositions or on the basis of heterogeneous component approaches. Homogeneous approaches have the advantage that they are generally easier to implement, but their performance is often limited to individual functionalities enabled by a single type of material. In contrast, heterogeneous concepts have a significantly greater development and optimization potential. For example, quantum emitters, low-loss WGs and efficient single-photon detectors made of different materials can be combined on a chip in front of fully integrated solutions. The chapter closes with an outlook in section 1.6 on future developments and challenges to be solved towards fully integrated IQPCs with full quantum functionality and a summary of the chapter.

1.2 NUMERIC MODELING AND OPTIMIZATION

This section discusses numerical methods that are used for the design and optimization of WG systems. The focus is on systems with integrated quantum emitters, in which the coupling efficiency between emitter and WG is usually the figure of merit. For instance, the chiral light-matter interaction can be maximized to yield directional light coupling into WGs at certain emitter positions. Further examples of numerical optimization are maximizing the photon extraction efficiency via grating couplers normal to the surface or lateral coupling elements and improving the structural design of nanocavities to maximize their quality (Q) factors. Typical numerical approaches that are used here are the finite difference time domain (FDTD) and the finite element method (FEM) concepts.

1.2.1 Finite Difference Time Domain

The FDTD method [181] is one of the most popular methods for electromagnetic simulation, and is currently available from multiple commercial as well as open sources [116]. As the name indicates, the method solves Maxwell's equations in time-domain and in three-dimensional space, allowing straightforward simulation of general, complex electromagnetic and photonic devices with a great degree of detail.

Starting from the differential form of the equations, both time- and space-derivatives are approximated with a finite differences scheme in a spatio-temporal grid. The standard grid, used in most implementations of the method, is generated from the so-called Yee cell [181], defined such that the electric and magnetic fields are staggered in time and in space, and sampled at spatial locations offset by a half pixel. Such a prescription allows space- and time-derivatives to be expressed in the center-difference scheme [181, 116].

The method allows almost arbitrary geometries to be defined by assigning spatially varying electric permittivity ($\epsilon(\mathbf{r})$) and magnetic permeability ($\mu(\mathbf{r})$) values across the grid. Importantly, because the discretization grid is regular, mesh refinement is not as flexible and efficient as in the FEM approach. Nonetheless, simulation of dispersive, anisotropic, nonlinear and time-varying materials is possible. The spatially finite computational domain can furthermore support a variety of boundary conditions (e.g., perfect electric or magnetic conductor, symmetry conditions, etc.), and open boundaries can be implemented by introduction of perfectly-matched layers (PML). A PML is a finite, absorptive electromagnetic medium that is placed side-by-side with the computation domain, while being matched to it. The matching condition means that waves emanating from the computation domain are not reflected at the PML interface, such that the latter, being sufficiently thick to absorb the wave completely, emulates an infinite half-space. The FDTD method allows excitation of electromagnetic structures with time-varying, spatially distributed electric or magnetic current sources, as well as with illumination field distributions, such as plane waves, Gaussian, beams and WG modes. In general, the temporal shape of the excitation source determines the spectral range over which the simulation is valid. Importantly, a minimum time-step length must generally be met, depending primarily on the spatial discretization with respect to the wavelength, though also on boundary conditions and material properties, in order to ensure stability of the simulation.

In an FDTD simulation, the electromagnetic field is obtained from the previous time-step over the entire computational domain, so that computation of relevant quantities such as electric and magnetic energy densities, Poynting vector, absorbed power, etc., at each time step is also possible. FDTD is commonly used for the calculation of resonant cavity modes [186]. Typically, a point-dipole source with a short temporal envelope is placed within the cavity, and illuminates it with a broad range of frequencies. If the cavity supports a resonance at a particular frequency within the range, it will be excited by the source. The time-

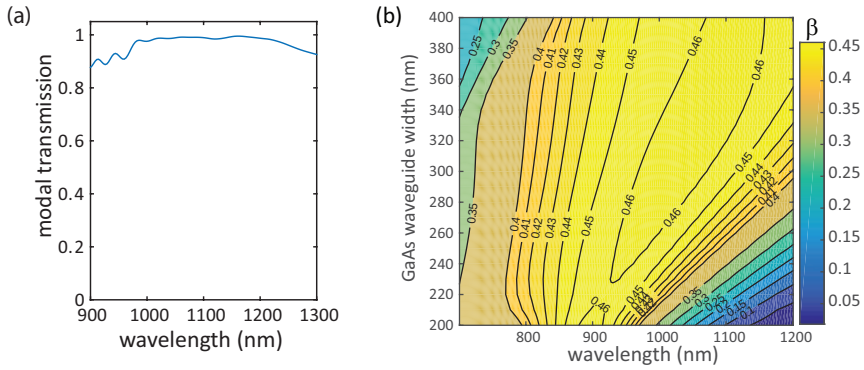

FIGURE 1.1 Examples of FDTD simulation results. (a) Modal transmission for the mode transformer from ref. [23], illustrated in Fig. 1.20(c). (b) Fraction β of the total power emitted by a dipole in the hybrid WG of Fig. 1.20(a), coupled into the fundamental TE mode for the hybrid WG of Fig.1.20(b). *(Reprinted from ref. [23] with permission from Springer Nature.)*

evolution of the cavity field in this case will display a sustained oscillation at the resonance frequency, with an exponential decay associated with energy escape from the cavity, and corresponding to its quality factor. In the frequency domain, this decay appears as a Lorentzian peak centered at the resonance frequency.

In contrast with frequency-domain methods, FDTD can allow the determination of the spectral response of a simulated system, within a specified frequency range, with a single run. After completion of the simulation, the time-dependence of the electromagnetic field and derived quantities can be converted to the frequency domain via Fourier transformation and normalization by the time-varying excitation source's spectrum. As an example, Fig. 1.20(c) in Section 1.5 shows the steady-state, simulated electric field amplitude for the on-chip adiabatic mode transformer demonstrated in ref. [23], at a single wavelength. The mode transformer consisted of a GaAs ridge stacked on a Si_3N_4 ridge, both of which featured a width taper along the propagation direction. The simulation consisted of launching the hybrid WG mode shown in Fig. 1.20(a) at the device input, and calculating the power delivered to the mode shown in Fig. 1.20(c) at the output. Figure 1.1(a) shows the calculated modal conversion spectrum for the structure, obtained from a single simulation run. As another example, Fig. 1.1(b) shows results of a simulation of an electric point dipole radiating at the center of the GaAs ridge in Fig. 1.20(a). Here, the fraction β of total emitted dipole power that couples to the TE mode shown in Fig. 1.20(a) is plotted as a function of wavelength and GaAs ridge width. The wavelength dependence here was obtained by Fourier transforming the time-dependent electromagnetic field for each dipole position.

1.2.2 Finite Element Method

In the case of FEM simulations, the Maxwell equations are solved under boundary conditions that are given by the device geometry, see e.g. Ref. [126]. Suitable source terms can be taken into account that approximate the emission properties of quantum emitters. The given problem is subdivided into finite elements, or small, easy-to-handle domains with locally defined boundary conditions and polynomial field-approximating basis functions. Taken together, finite element piecewise-continuous field solutions can be obtained for the entire domain. Common examples of finite elements are triangles and rectangles in 2D and tetrahedrons and cubes in 3D, see e.g. Fig 1.3(b). In modern FEM solvers, the meshes that define these domains are dynamically adjusted during the calculation in order to adapted to the multi-scale properties of the photonic structures and to minimize the necessary computing time for a given computational accuracy. Before calculating solutions of the problem, these domains are pieced together in a way that tangential continuity of the electric and magnetic field across the boundaries of neighboring patches are ensured. Noteworthy is that fact that, while FEM applies a discretization to the geometry, it does not use any approximation to Maxwell's equations themselves. In fact, it approximates the solution space in which one seeks a reasonable approximation to the exact solution. Advantages of the FEM concept include the accurate treatment of complex geometrical shapes, a flexible and iterative refinement of the finite element mesh by considering details of intermediate solutions, and the availability of high order approximations to ensure fast convergence. Overall, FEM constitutes a likewise flexible and powerful concept to numerically model to optical properties of nanophotonic devices and integrated photonic circuits.

To illustrate and underline the suitability of FEM for the numeric optimization of photonic WG systems, we present results on chiral light-matter interaction and directional coupling in QD based ridge-WG circuits. We consider a GaAs based ridge WG system as an easy-to-fabricate model system for the studying and maximizing the directional emission of a quantum emitter coupled to confined modes in the WG, where the lateral displacement of the emitter Δx acts as parameter. The layer design includes a lower AlGaAs/GaAs distributed Bragg reflector (DBR) to reduce photon losses into the substrate and GaAs capping layer which includes the quantum emitter at the vertical field maximum of the WG modes, see Fig. 1.2(a). The computational geometry is shown in panel (b) which also indicates the used mesh and coordinates. A FEM solver was used to calculate the propagating eigenmodes for a WG width of 850 nm and a height of 800 nm at a wavelength of 930 nm. The corresponding electric field distributions $I = |E_x|^2 + |E_z|^2$ are presented in Fig. 1.2(c) for modes TE_0 and TE_2, where the different mode index is clearly reflected in the corresponding mode pattern. Beyond the simple calculation of intensity profiles, FEM modeling also provides additional information like on the corresponding degree of polarization. This aspect is presented in panel (d), where the degree of circular polarization

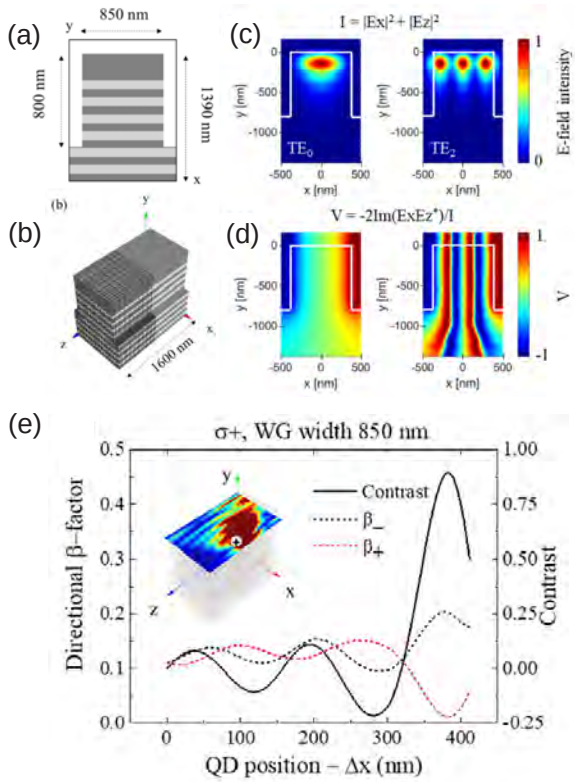

FIGURE 1.2 Numeric device modeling using the FEM approach. (a) Cross-section of the considered ridge WG system. The WG has a width of 850 nm and the layer design consists of lower DBR with 8 AlGaAs/GaAs (dark grey/grey) mirror pairs followed by 230 nm of GaAs (dark grey), which includes the QD layer (not shown). (b) 3D representation of the considered model structure including information about the used computing domains. Calculated intensity distributions (c) and degree of circular polarization (d) for the fundamental and a 2nd order TE-like mode. (e) Calculated quantum emitter coupling factors $\beta_{\pm}$ to modes traveling in the ±z direction, and directionality contrast as a function of lateral emitter displacement Δx. Inset: Visualization (cross-section) through the electric field distribution for the dipole placed at $\Delta x = 350$ nm. *(Reprinted from ref. [107] with permission from American Chemical Society.)*

$V = -Im(E_x E_z^*)/I$ is plotted in the cross-section of the considered WG geometry for modes TE_0 and TE_2. While for the mode TE_0, a continuous transition from negative to positive values of V and oscillatory behavior are observed for and TE_2. It turns out that this oscillatory behavior of the circular polarization together with the peculiar mode profile of the TE_2 leads to pronounced chiral light-matter interaction as quantified in the directional β-factor $\beta_\pm = \frac{\gamma_\pm}{\gamma_+ + \gamma_- + \Gamma_{\text{out}}}$ with the decay rates $\gamma_\pm$ into left and right propagation modes and Γ_{out} the residual recombination rate by all other channels including losses due to non-guided modes and non-radiative intrinsic recombination, and the directionality contrast $C = \frac{\gamma_- - \gamma_+}{\gamma_- + \gamma_+}$ [89]. Both parameters are plotted in Fig. 1.2(e) for TE_2 as function of the emitter's lateral displacement Δx and show an oscillatory behavior with maximum directionality at an emitter position close to the edge of the WG, i.e. at $\Delta x \approx 380$ nm [107]. Thus, the numerical modeling here shows the existence of a chiral point near the edges of the WG, for which directional emission is maximized, thereby establishing a design rule to maximize the directionality of emission, in good agreement with experiment as presented in Sec. 1.4. This example nicely illustrates the power of the FEM approach to support the design of quantum devices to obtain optimum performance with regard to the desired functionality. Noteworthy is the fact that FEM simulations are also very beneficial to maximize the photon-coupling and outcoupling efficiency of photonic quantum devices [48, 41, 157, 176, 175].

1.2.3 Comparison of finite element method and finite difference time domain approaches

Nanoresonators based on PC membranes form an interesting system for comparing different numerical methods. In Ref. [25], this was carried out for FDTD and different FEM approaches, as well as for finite-difference frequency-domain (FDFD), the aperiodic Fourier modal method (aFMM) and the surface integral equation (SIE) approach, in which resonance wavelengths and Q-factors for L5 and L9 cavities were calculated and compared. Here in the case of L5 and L9 cavities, which can act as integral parts of IQPCs, 5 and 9 holes are left out of the periodic lattice of holes, see Fig. 1.3(a), in order to localize light in the resulting photonic defects. The calculation of the Q-factors represents a significant computational challenge, which requires a 3D calculation in the system under consideration. Furthermore, the Q-factor describes optical losses to the environment, which cannot be taken into account directly in common models and is usually approximated by absorbing boundary conditions in terms of PLMs [9], whereby the choice of the computational domain can affect the result in an uncontrolled way [25].

The main results of comparison between the above mentioned numeric methods are summarized in Fig. 1.3(c) which summarizes the calculated resonance wavelengths λ and Q-factors for the considered L5 and L9 cavities. It is seen that all methods, apart from aFMM, approximate the average values (green lines)

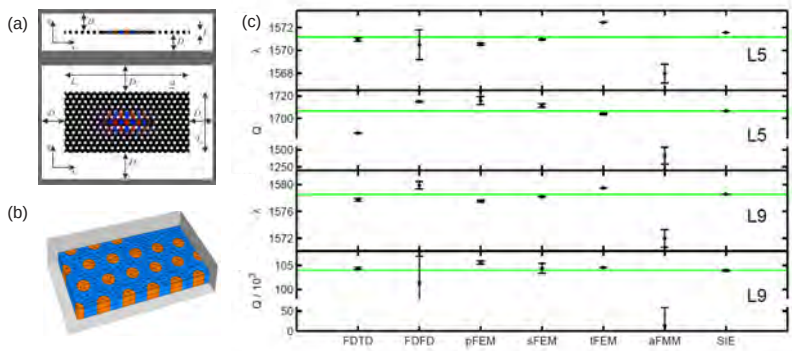

FIGURE 1.3 Schmatic illustrating the PhC membrane geometry and the electric field E_y profile for the M1 mode in an L9 cavity in the $y = 0$ (top) and the $z = 0$ (bottom) plane of the structure, respectively. (b) Computational mesh of the L5 PhC geometry used in the scattering analysis FEM (sFEM) simulations. (c) Comparison of the resonance wavelength and the Q-factor for an L5 and an L9 PC cavity. The green horizontal lines indicate the averaged values and vertical bars the numerical error. The required computational time was in the range of 3 (FDFD) to 146 (aFMM) minutes. *(Reprinted from ref. [25] with permission from Optical Society of America.)*

quite well. However, it is interesting to note that the given error bars are to small to account for the deviation of the different method's results from the average value. In other words, it seems that the used methods underestimate the numeric error, an aspect which one should have in mind when interpreting the obtained results. Moreover, the comparison yields that for the particular problem, the SIE method provides the most accurate results.

Overall, the presented numerical methods and the results shown give an impression of their remarkable level of development and of the possibilities that result in particular for the design optimization of nanophotonic elements and especially IQPCs. Current and future developments can use machine learning approaches to achieve a further increase in efficiency and computing accuracy using e.g. Bayesian algorithms. In addition, it will be interesting to integrate more precise descriptions of the quantum emitters beyond simple dipole models in the simulations and to take quantum effects into account.

1.3 FABRICATION TECHNOLOGIES

IQPCs are highly optimized components, the manufacture of which requires sophisticated and precise methods of modern nanotechnology. IQPCs are usually realized on single-crystalline planar semiconductor structures mainly based on silicon and III-V compound semiconductors, as well as combinations thereof. These materials are structured using metal and dielectric layer deposition, lithography and etching processes with nanometer precision in order to achieve the

desired functionality. Furthermore, they can be combined with other materials e.g. via wafer bonding in heterogeneous approaches, so that complex, fully integrated quantum circuits are created. This section provides an overview of common and advanced manufacturing processes for the implementation of highly functional IQPCs. The focus is on modern technology processes such as in-situ lithography that were specially developed for structuring IQPCs with integrated quantum emitters. The fabrication aspects presented here are taken up again in the following sections 1.4 and 1.5, in which the specific requirements and physical-technical properties of the circuits as well as their physical properties are discussed.

1.3.1 Realization of planar substrates for integrated quantum photonics circuits

Silicon-based IQPCs are usually realized on high-purity single-crystal silicon, as used for highly integrated electronic circuits. Single-crystal silicon is produced through crucible processes and made available as planar wafers for the further processing of IQPCs. The desired functionalization is achieved essentially via lateral structuring in combination with deposition of further materials. We refer to Ref. [102] for further details on the very established production of silicon-based substrates.

Optically active III-V compound semiconductors with a direct band gap are of high interest for the development of IQPCs. GaAs and InP semiconductors in particular are characterized by excellent optical properties. They have a pronounced optical nonlinearity as the basis, for example, for quantum frequency conversion in customized WG structures [18] and integrated photon-pair generation [64]. In addition, self-organized InGaAs QDs form the basis for state-of-the-art single-photon sources with record values in terms of the single-photon emission rate [150], the single-photon purity [162] and the photon indistinguishability [194]. Corresponding planar wafers are realized on the basis of single-crystal GaAs substrates through the epitaxy of semiconductor heterostructures. For this purpose, the methods of molecular beam epitaxy (MBE) and metal organic chemical vapor deposition (MOCVD) are used. Both make it possible to achieve single-crystal layers with atomically precise interfaces, tailored layer sequences and the highest optical quality. With regard to IQPCs, layer sequences that contain QDs as single-photon emitters are of particular interest. These are usually integrated into the semiconductor heterostructures using the Stranski-Krastanov process. For example, InGaAs QDs are created in a GaAs matrix. The quantum emitters thus achieved form almost ideal two-level systems with narrow emission line preparation in the range of the homogeneous linewidth and quantum efficiencies beyond 90 % as the basis for quantum optical applications [81]. However, the self-organized manufacturing approach has an adverse effect on the further processing. The random position and spectral position of individual QDs prevent scalable component production using common

lithography processes. This has motivated the development of deterministic manufacturing concepts, which are presented in Sec. 1.3.2.

1.3.1.1 Wafer Bonding

We next discuss the wafer bonding technique, which is of particular importance for the realization of hybrid or heterogeneous photonic circuits to be presented in section 1.5. While QD lasers produced on silicon substrates through a direct wafer fusion bonding process were demonstrated [37], in Ref. [23] it was shown that direct wafer bonding could be leveraged to produce SiN WG-based photonic circuits incorporating single QDs as single-photon sources. In this method, two wafers of different materials are initially brought together and bonded to form a heterogeneous wafer stack. Typically, the substrate of one of the wafers is removed, leaving behind a thin film of material that can be processed alongside the receiving material substrate. Device fabrication can then follow a single high-throughput process flow with completely top-down techniques, where different material layers are subsequently etched, following high-resolution lithography. The fully top-down fabrication process, which allows high-resolution lithography-based definition of the IQPC geometries of all layers involved, in principle allows fabrication of high performance geometries.

One of the main advantages of such an approach is in scalability - it allows wafer-scale device production by leveraging the massive parallelism enabled by mature, top-down semiconductor fabrication methods. Indeed, the wafer bonding approach has been employed commercially for the creation of heterogeneous integrated III-V semiconductor/silicon-on-insulator photonic devices, such as lasers and transceivers, with optical gain provided by III-V materials [79].

An important issue with the wafer bonding approach is that considerable effort is required for bringing two materials together before device fabrication can even be considered. After the two materials are bonded, sub-optimal device performance may still arise due to process incompatibility. Increasing the complexity to more than two types of materials on one chip is furthermore challenging. At least for fast device prototyping, determinsitic fabrication methods presented in the following section offer advantages over wafer bonding.

1.3.2 Deterministic fabrication technologies for quantum circuits with integrated quantum emitters

The implementation of fully functional IQPCs usually requires the monolithic integration of individual quantum emitters as active elements. For example, applications in the field of boson sampling would benefit enormously if the input state based on individual photons could be generated directly on-chip. So far, this has not been possible and external single-photon sources are used in combination with complex multiplexing [188, 91, 190]. This limitation can be explained by the fact that high-quality quantum emitters such as nitrogen-vacancy (NV) centers

N \ QD Density (cm^{-2})	Random yield $P_{N,rdm}$			Deterministic yield P_N		
	10^7	10^8	10^9	10^7	10^8	10^9
2	0	0.02	0.17	0.99	1	1
3		$<10^{-3}$	0.03	0.94		
4		0	0.005	0.83		
5			$<10^{-3}$	0.66		
6			$<10^{-3}$	0.49		

FIGURE 1.4 Estimated process yield per write field for fabricating a WG structure with N QD nodes that are all within a resonance tuning range of 1 meV. A 50 x 50 mm^2 deterministic preselection field and a 100 nm x 10 mm (parallel and normal to the WG) spatial positioning tolerance is assumed. Values < 10−4 are rounded to 0 and > 0.9999 rounded to 1. *(Reprinted from ref. [152], Supplementary Information.)*

in diamond or semiconductor QDs in solid-state systems are usually realized in a self-organized way. As a result, their positions and their emission energies are not predetermined, so that the process yield using conventional nanostructuring methods is very low and prevents a scalable production of IQPCs. This is mainly explained by the fact that, for advanced applications, a given number N_{QE} of quantum emitters with the same emission energy on the scale of the homogeneous linewidth (approx. 1 μeV) have to be integrated precisely into the WG.

To clarify this aspect, the table in Fig. 1.4 compares the expected process yield for the integration of multiple QDs in WG systems using conventional lithography and deterministic in-situ lithography. The underlying estimate assumes that the QDs are self-organized with a specified areal density and an inhomogeneous broadening of the ensemble emission of 50 meV which is typical for In(Ga)As QDs. Furthermore, spectral fine tuning in a range of 1 meV for individual QDs is included, for example via Stark tuning [118], in order to achieve spectral resonance of the QD emission. From these considerations, which are described in Ref. [152] (Supplementary Information) and summarized in Fig. 1.4, it becomes clear that deterministic manufacturing processes are far superior to conventional methods and that it is only likely that the necessary scaling can be achieved using them. The process yield of conventional lithography is almost zero for integration of two QDs and a low QD areal density of $10^7 cm^2$. It can be increased by a higher areal density, but even with a density of $10^9 cm^2$, the process yield for the integration of 6 quantum emitters is below 0.1 %. Areal densities of this size, however, result in a large number of QDs that were not intentionally integrated, which has a disadvantageous effect on the single-photon purity and can also lead to absorption losses. In contrast, deterministic methods promise almost perfect process yields at a QD area density of $10^8 cm^2$ and up to 50 % at $10^7 cm^2$, which illustrates the enormous advantages of such methods.

Deterministic manufacturing processes for quantum devices essentially include the positioned growth or the positioned implantation of quantum emit-

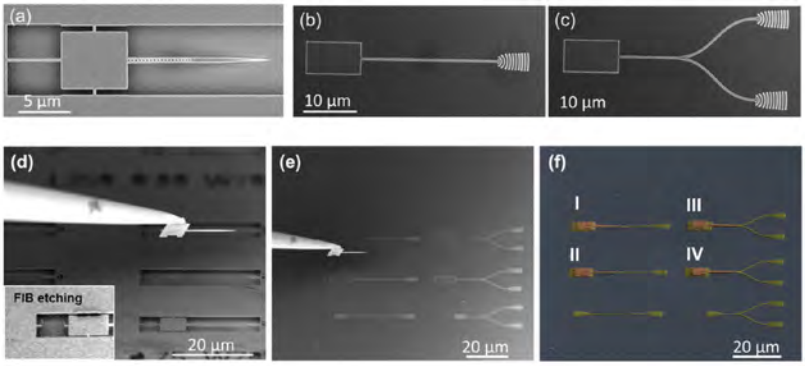

FIGURE 1.5 Pick-and-place technique for the deterministic realization of IQPCs: (a) SEM image of a tapered InP nanobeam containing InAs QDs. (b,c) SEM images of WG structures in silicon. The square pads at the nanobeam's left end are used for placing the InP nanobeam. (d to f) Presentation of the pick-and-place procedure which uses a microprobe tip combined in an SEM equipped with a FIB unit to place InP nanobeams with InAs QD onto Si WGs. *(Reprinted from ref. [76] with permission from American Chemical Society.)*

ters, so-called pick-and-place techniques and deterministic lithography processes [142]. In this context, the positioned growth, for example via nanohole arrays as nucleation sites, and to a certain extent also the positioned implantation of quantum emitters have the disadvantage that the spectral position of the quantum emitters is not controlled, so that there is still no high scalability. In contrast, quantum emitters with desired spectral properties can basically be selected from a large pool of conventionally produced structures in the pick-and-place process. However, this can lead to a large overhead of potentially unusable quantum emitter structures. Alternatively, in deterministic lithography processes, suitable quantum emitters are selected on the basis of their emission intensity and their spectral properties, in order to, then, define and produce the desired nanophotonic structure with nanometer accuracy around them.

Pick-and-place and transfer techniques

In the pick-and-place [106, 200, 33, 76] and transfer-printing [72, 73] approaches, which are of particular importance for heterogenous IQPCs (see section 1.5), different components of a device, composed of different materials, are produced separately and in parallel through well-developed fabrication techniques, and then brought together through a low-throughput mechanical transfer process. As an example, in Ref. [106] integration of quantum memories based on NV center defects in etched diamond nanobeam WGs onto SiN WGs was demonstrated using a pick-and-place process that employed micro-manipulation of tungsten tips. The same technique was also used in Ref. [111] to demonstrated the integration of niobium nitride superconducting nanowire single-photon detectors (SNSPDs), produced on SiN membranes, over an silicon-on-insulator (SOI) -

based photonic circuit. Pick-and-place with tungsten tips was also used in Ref. [200] and [34] to integrate single-photon sources based on InP nanowires with embedded InAsP QDs into a SiN photonic circuit. In Ref. [72], InAs quantum dot-containing GaAs nanobeam photonic crystal cavities evanescently coupled to underlying GaAs WGs were produced through a transfer-printing process. Here, a polydimethylsiloxane (PDMS) stamp was used to lift suspended GaAs nanobeams from a processed GaAs wafer. The destination substrate consisted of GaAs-on-SiO_2 wafer onto which GaAs ridge WGs were etched, covered by a spin-on-glass (SOG) top cladding.

In [76] the pick-and-place technique was used to realize heterogenous QD-WG systems. Here InGaAs QDs are integrated into photonic membrane structures using conventional lithography methods. Low loss Si WG structures are structured in parallel. Subsequently, the quantum emitters are spectroscopically characterized and membrane structures with the desired optical properties are selected. In order to realize the heterogeneous QD WG structures, suitable QD membrane structures are detached from the carrier material (GaAs) using focused ion beam (FIB) technology and are transferred using a pick-and-place technique by a microprobe tip with high accuracy to selected positions on the silicon WG structure, see Fig. 1.5. IQPCs can thus be implemented with high-quality quantum emitters, low optical losses and high design flexibility. However, many QD membrane structures have to be generated and elaborately pre-characterized in order to select elements with the desired optical properties. Furthermore, the pick-and-place process is rather tedious, time-consuming and difficult to automate.

Overall, the pick-and-place and transfer printing techniques offer a lower barrier for creating maximally performing devices based on components fabricated with low-yield processes, by allowing pre-screening and selection of the best performers within a population. For instance, such capability was leveraged in the diamond NV center quantum memories in Ref. [106], given that consistent, desired spectral and spin properties of fabricated nanobeams with inhomogeneous populations of NV centers are difficult to achieve. Similarly, Ref. [111] reports on an integrated photonic circuit chip for photon correlation measurements, containing 10 low-jitter SNSPD detectors with consistent timing jitter and detection efficiencies. With pick-and-place and transfer printing, greater scalability is sacrificed in favor of processing flexibility and fast turn-around. Because finalized heterogeneous photonic chips are processed in separate runs, fewer issues with process compatibility can be expected, in comparison with a wafer bonding. This endows the techniques with a great degree of flexibility, offering a low barrier towards the incorporation of different types of materials together. While the technique is particularly attractive for rapid device prototyping and proof-of-principle demonstrations, agile automation can potentially lead to significant gains in device scalability. Importantly, however, the lack of deterministic control over self-assembled QD growth location is, similar to the wafer bonding approach, a challenging scalability bottleneck for pick-and-place

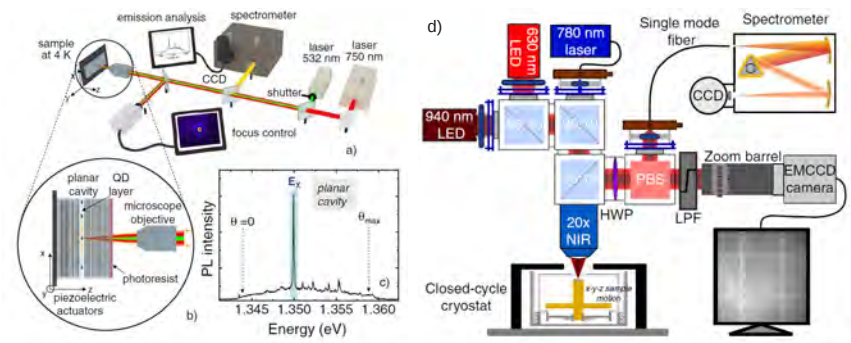

FIGURE 1.6 In-situ optical lithography performed at 10 K and photoluminescence (PL) imaging as deterministic tools for QD device processing. (a) Schematic view of the in-situ optical lithography setup including two lasers used for PL registering (red laser) and optical lithography (green laser). (b) Zoom-in view illustrating the selection of suitable QDs via the red laser and the patterning of the device cross-section into UV resist with the cross-section aligned to the QD position by the green laser. (c) Low temperature PL spectrum of planar microcavity sample. Emission of a selected QD is marked (E_X). (d) Schematic view of the PL imaging set-up. The sample is illuminated by an infrared LED and either a red LED or a 780-nm laser is used for wide-range and local excitation of QDs, respectively. PL imaging and QD registering relative to alignment markers are performed by detecting the emitted and reflected light by an electron-multiplied charge-coupled device (EMCCD) camera. Spectral information is obtained by a grating spectrometer. Subsequent to the PL imaging nanophotonic structures are patterned by conventional EBL using the alignment markers to place these structures with high accuracy preregistered QDs. *((a), (b), (c): Reprinted from ref. [30] with permission from American Physical Society. (d) Reprinted from ref. [148])*

based device fabrication.

In-situ lithography techniques

As an alternative concept, deterministic in-situ lithography has been developed in the past ten years and is now an important tool in the field of quantum nanophotonics. In 2008, the optical in-situ lithography was pioneered [30] and has been used very successfully for the deterministic realization of QD micropillars as single-photon sources [169, 184]. Here, for optimal performance of the single-photon sources, the QD must be in spectral and spatial resonance with the resonator mode. To ensure this, the surface of a planar microcavity sample is first scanned with a low-energy (red) laser in a photoluminescence scan and the positions of QDs with a suitable spectral position are determined, see Fig. 1.6(a). In the following lithography step, the desired structure, here a micropillar, is defined via a green laser in a UV-sensitive resist precisely aligned to the position and with its diameter matched to ensure spectral resonance with the pre-selected QD. The UV resist is spin-coated in advance and the entire process is carried out at cryogenic temperatures to ensure a sufficiently high emission intensity of the QDs. An attractive variant of this method is based on a two-stage process in which the positions of suitable QDs are first determined relative

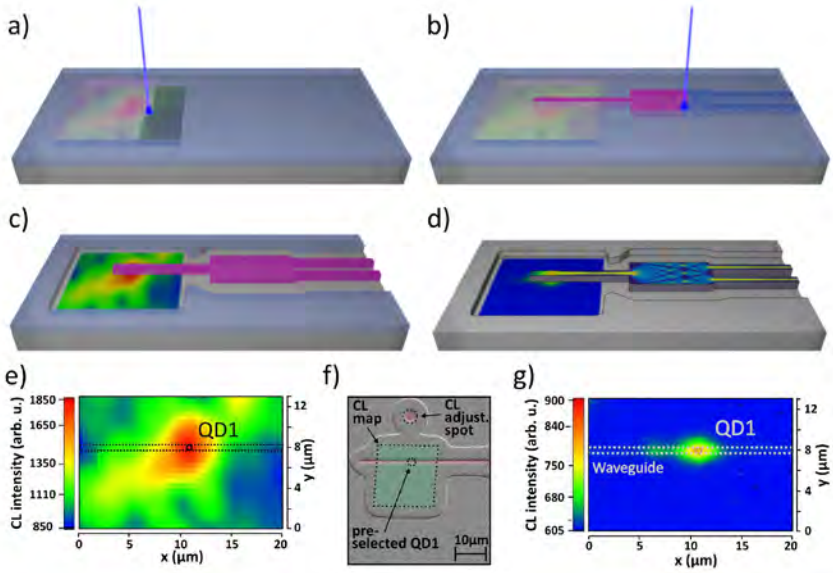

FIGURE 1.7 In-situ electron-beam lithography of IQPCs. The process is performed in a customized SEM which includes a CL unit, a He flow cryostat and an EBL pattern generator. (a) Selection of suitable QDs by CL registering at low electron-beam dose at 10 K. (b) In-situ EBL at 10 K to integrate selected QDs into ridge WGs and to pattern also more complex WG structures such as MMIs at electron-beam dose. (c) Schematic of the sample after the subsequent development process in the cleanroom. The locally inverted electron-beam resist (magenta) acts as etch mask in the following plasma etching process (d). CL map obtained during QD registering (e), SEM of a fully processed device (f) and CL map showing emission of a QD deterministically integrated into a ridge WG (g). *(Reprinted from ref. [152] with permission from American Chemical Society.)*

to alignment markers and then, after the mark detection, the desired structure is defined by means of electron beam lithography [148, 88], see Fig. 1.6(b). This process benefits from the significantly higher resolution of electron beam lithography (EBL) compared to optical lithography in the original process, where the higher resolution is strictly required for the realization of WG circuits with feature sizes well below the resolution of optical lithography. However, the two-stage process is technically much more complex.

To combine the advantages of in-situ lithography and the high flexibility and resolution of EBL a further technique was developed and named in-situ EBL [47]. This deterministic nanofabrication technology platform applies low temperature cathodoluminescence (CL) spectroscopy to find select suitable QDs via convenient 2D scanning, and then performs low temperature EBL using the same scanning electron microscope (SEM) system. The structuring benefits from the highly optimized scanning properties of the SEM or CL technology and uses the enormous advantages of the EBL in order to produce quantum devices of the highest quality in a precise and flexible manner [49, 50, 154, 69]. The

in-situ EBL technique has been refined more and more in recent years and has been used very successfully and in many ways for the implementation of efficient single-photon sources, for example based on microlenses [68, 151, 48, 59]. With regard to the development of IQPCs, in-situ EBL has the great, if not decisive, advantage over in-situ optical lithography that, thanks to the extremely flexible and high-resolution EBL, it can also write very complex structures with the finest structural details. In particular, the in-situ EBL technology has succeeded in integrating InGaAs QDs deterministically into GaAs WG structures and expanding them into more complex units including e.g. multi-mode interference (MMI) beamsplitters [152, 107, 155].The corresponding process flow is shown in Fig. 1.7. Panel a) shows the 2D scanning of the QD sample using CL spectroscopy using a low EBL dose (typically performed at 10 K). The EBL positive resist (PMMA or CSAR) is already on the sample surface and is homogeneously exposed in this step in parallel to finding suitable QDs. Immediately afterwards, the desired WG structure is precisely written into the resist with a high EBL dose as shown in panel b). Furthermore, elements of the intended IQPC such as beamsplitters (here a MMI coupler) and possibly also output ports are defined in the resist (also at 10 K). The EBL dose is chosen so high that the resist is locally cross-linked again in negative-tone resist mode. After development in the clean room the inverted remaining resist acts as an etching mask (see panel c)) in a plasma etching step in which the written structure is transferred to the semiconductor (see panel d)). The real process flow is further illustrated by panels e) -g). Panel e) shows a 2D CL map recorded in the first in-situ EBL step to select a suitable QD with a suitable spectral features and high CL intensity, which is marked here with QD1. Panel f) shows an SEM image of a processed QD-WG element, in which the position of the previously selected and deterministically integrated QD (QD1) is marked. The 2D CL map in panel g) was recorded for process control and demonstrates impressively that the QD was successfully integrated into the QD at the planned position. Furthermore, all other emission centers were eliminated in the etching step that removes the semiconductor material including the QD layer away from the WG. By using the inverted resist as an etching mask, the process described is overall very simple, reproducible and robust. It basically allows a very scalable production of IQPCs and can also be used, for example, to interface superconducting single-photon detector elements with high precision and alignment accuracy with QD WGs.

1.3.3 Etching and processing technologies for integrated quantum photonic circuits

After the production of the starting materials and the lithography of the nanophotonic elements, the actual structuring of the IQPCs is carried out. In the simplest case, this only involves the etching of WG structures. However, complex manufacturing processes can also be involved, for example to manufacture heterogeneous IQPCs based on different materials or fully integrated circuits. An

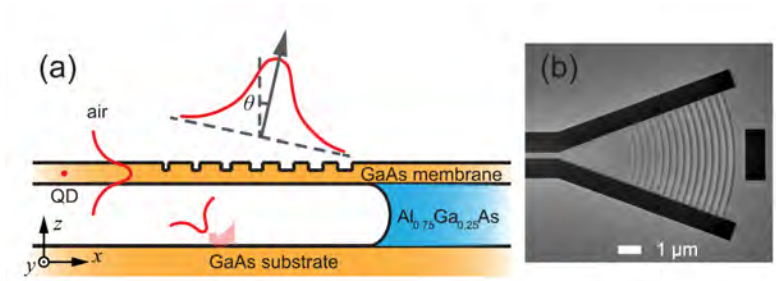

FIGURE 1.8 IQPC based on GaAs membranes. The structure is realized by a combination of dry etching (ICP-RIE) and wet chemical etching. (a) Schematic cross-section of the GaAs membrane with integrated shallow-etched grating couplers. (b) SEM image of the fully processed structure. *(Reprinted from ref. [202] with permission from American Institute of Physics.)*

overview of the most important process technologies is given below.

Etching of cavity and WG structures

The most common method for realizing photonic WG structures is reactive-ion etching (RIE). Here, the semiconductor material is removed physically and often also chemically supported in areas that are not protected by etching masks. As mentioned above, when describing the in-situ EBL process, cross-linked resist can be used as etch mask, however, most often so-called hardmasks, such as Si_3N_4, SiO_2, or metals, are used to improve the selectivity of small features. Here, in contrast to wet chemical etching, dry plasma etching enables a very anisotropic etching pattern, which is essential for WGs. In some cases, combinations of the two etching processes are also used, for example to implement membrane structures.

As an example in Fig. 1.8, a GaAs membrane structure with InAs QDs is shown, which contains a grating outcoupler for the light decoupling normal to the surface [202]. The structure was grown using MBE and defined using conventional EBL. As can be seen in partial image (b), the layer structure includes the actual (160 nm thick) GaAs membrane structure (with InAs QDs in the center) as well as a 1350 nm thick $Al_{0.75}Ga_{0.25}As$ layer, which acts as sacrificial layer when realizing the membrane structure.

The fabrication process to realize the membrane structure involves two EBL steps followed by dry etching. First, the grating grooves are written and etched using low-power BCl_3/Ar RIE. In the second EBL step the WGs and focusing tapers are defined with high accuracy to the grooves, before BCl_3/Cl_2/Ar supported inductively coupled plasma RIE (ICP-RIE) is used to remove the desired semiconductor material. It is important to note that this RIE essentially exposes the structures of the upper GaAs layer and that the actual membrane structure is realized in the following wet chemical process step. In this step, the locally exposed $Al_{0.75}Ga_{0.25}$ As sacrificial layer is removed selectively by means of HF

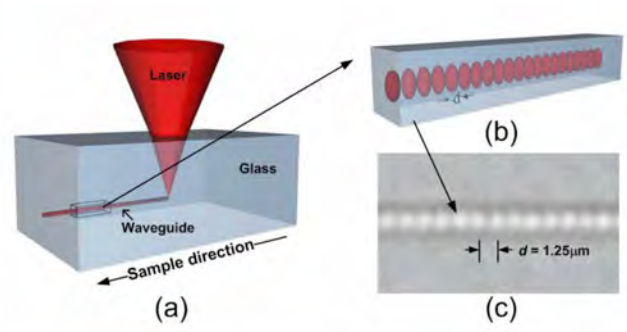

FIGURE 1.9 Illustration of direct 3D fs-laser writing WGs in fused silica. (a) High light intensities of a fs-laser in the focal region of the writing objective break the SiO_2 bonds in fused silica which leads to a locally increased refractive index after densification. (b) In the writing process, the WG (with higher refractive index) is created by moving the sample relative to the focus point of the laser in a spot-like fashion, which results in isolated modification volumes forming the desired WG (c). *(Reprinted from ref. [201] with permission from Optical Society of America.)*

etching below the previously dry-chemically etched areas, so that the partially suspended GaAs membrane is formed [105]. The latter process is often combined with CO_2 critical point drying in order to reduce mechanical stress on the fragile WG structures [84]. Alternatively, hydrogen fluoride vapor etching can also potentially be used. Such a process has been employed to remove oxide sacrificial layers in ref. [26], to create high quality factor silicon-on-insulator photonic crystal nanobeam cavities. This example shows in an impressive way how the sophisticated interaction between dry-wet chemical etching processes can lead to complex IQPCs.

Direct laser writing of photonic waveguide systems

An alternative method for producing photonic WG structures is direct laser writing [121, 100, 179]. In this process, 3D WG structures are flexibly and comparatively simply written optically with focused laser pulses in solid state materials. This means that optical circuits can be generated quickly and efficiently, for example to perform quantum mechanical simulations [121, 179], to implement boson sampling [182] and to study topological photonics [195].

Direct laser writing makes it possible to implement not only individual WGs, but, above all, arrays of WGs with high precision - for example in fused silica (SiO_2). Each WG can be structured individually, and modifications such as defects due to a local change in the refractive index can also be integrated. The basic idea is to first break molecular ring structures in fused SiO_2 locally using focused fs-laser pulses [201, 179]. The subsequent recombination leads to smaller ring structures, which in turn locally increases the refractive index and thus enables light guidance in WGs with suitable dimensions. The direct laser writing concept is shown in Fig. 1.9. In practice, WGs are manufactured

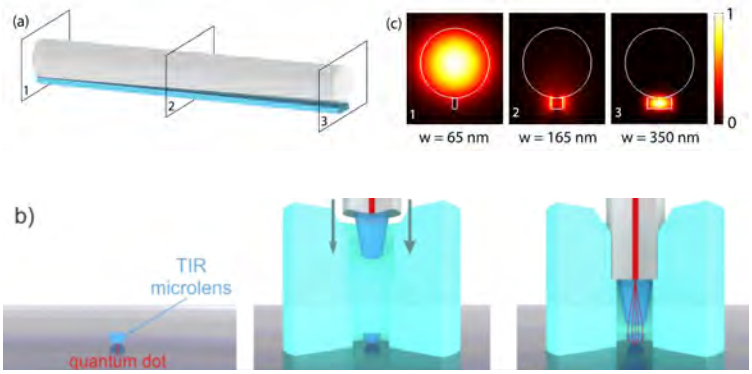

FIGURE 1.10 Direct fiber coupling of nanophotonic elements. (a) Schematic of a fiber-coupled WG system. The microfiber (gray cylinder) is brought into contact with the tapered GaAs WG to allow for efficient light coupling. (c) Normalized electric field amplitude $|E|$ plotted in the cross-section plane of the coupled WG system different WG widths w. (b) Illustration of the on-chip fiber-coupling using 3D printed micro-optics (a Total Internal Reflection (TIR) microlens) in combination with a corresponding microlens at the fiber-facet and on-chip fiber chuck. The 3D printed microlenses are shown in blue. *((a), (c): Reprinted from ref. [24] with permission from Optical Society of America.)*, (b): Reprinted from ref. [11].

using this method by continuously moving the material to be structured with the required accuracy relative to a focused laser spot. Here, highly complex 3D WG structures can be written using translations in all three spatial directions. The smallest structure dimension is essentially given by the size of the laser spot, of the order of a few μm. The refractive index contrast that can be achieved typically reaches values in the range of 10^{-3} and can be controlled by the writing speed. The resulting structures are permanent, require no further post-processing and have low optical losses in the range of 0.5 dB/cm. However, it is disadvantageous that structures of this type are purely passive and direct integration of active elements such as quantum emitters and detectors may be challenging.

1.3.4 Concepts for efficient photon outcoupling

The focus of IQPCs is on-chip processing of single photons. Nevertheless, the photon coupling and decoupling is of great importance. As long as there are no fully integrated IQPCs, for example, photons must be coupled in at the input ports and coupled out at the outputs for detection or for transfer to photonic networks. For this purpose, various approaches have been developed, which include grating outcouplers [38, 20, 87, 107] (see e.g. Fig. 1.8(a)) for photon extraction normal to the surface and adiabatic outcouplers for in-plane extraction [77].

The above-mentioned approaches to photon coupling are aimed primarily at proof-of-principle experiments on a laboratory scale and free-space optics. For

practical applications, however, it is crucial to connect IQPCs directly to optical fibers in order to avoid complex and fault-prone optical paths and to ensure user friendliness. The direct fiber-connection represents a major technological challenge, since IQPC elements and fiber optics, especially in case of single-mode fibers, have to be aligned with each other with sub-μm accuracy and have to be mechanically and thermally very stable due to the cryogenic operation of the sources. In addition, good mode matching must also be ensured for high coupling efficiency between IQPC and fiber. In Ref. [24], adiabatic-evanescent coupling between a tapered nanobeam WG and a microfiber was established for this purpose via an in-plane approach as shown in Fig. 1.10 (a, c). Here, high chip-to-fiber coupling efficiency was achieved, however, the fiber was not permanently connected to the IQPC. Concepts for permanent coupling between glass fibers and nanophotonic elements have already been established in superconducting detectors and use either high-precision mechanical elements or suitable adhesives. Current developments in the field of fiber-coupled single-photon sources are very promising and point the way to on-chip fiber coupling of IQPCs as well. The alignment between emitter and fiber is particularly challenging here, since QDs, for example, hardly emit any light at room temperature, which prevents active alignment based on the emitter signal. This issue was circumvented in Ref. [149] by using the local wetting-layer signal for alignment and subsequent gluing of a multi-mode glass fiber. In another very elegant method, the optical interference signal between a laser-illuminated glass fiber and the sample surface was used to determine the surface topography and to couple a single-mode glass fiber with gluing and sub-μm accuracy with a QD structure [203, 110]. A promising alternative to this, which is also very attractive for the fiber coupling of IQPCs, uses 3D printing of micro-optics and on-chip fiber holders to achieve an extremely precise and optically efficient connection between nanophotonic structure and glass fiber [10, 11], as presented in Fig. 1.10(b). The mentioned approaches are very promising for direct fiber coupling to IQPCs with grating outcouplers, towards modular devices for direct integration into quantum networks.

1.4 HOMOGENOUS WAVEGUIDE SYSTEMS

The integration of on-chip photonic quantum information processing has been developed on a variety of platforms and has benefited from very productive advances in the past decade. The simplest method was to integrate individual photon sources and elements of linear optics into a system that consists of single-material, or in other words homogeneous WGs. This was the first approach to implementing IQPCs. These successes were achieved using mainly already established manufacturing techniques developed for classical photonic chips. The problems of purity, decoherence, scalability and versatility of individual photons are very different depending on the material used. We give an overview of the recently developed and investigated platforms for the implementation of a

homogeneous IQPC. We discuss the strengths and weaknesses of the individual platforms. In particular, we will highlight the advances in silicon-based platforms, III-V semiconductors and diamond. So far, they are the most reliable and most advanced platforms for integrated quantum electronics with different strengths and weaknesses. In this section we only refer to WG-based structures made of naturally compatible materials (Si/SiO_2 or GaAs/AlGaAs/InGaAs) as opposed to hybrid platforms made of different material types, which have their own challenges and problems and are discussed in section 1.5. We conclude this section with a synthesis of the platform viability discussed as potential self-sufficient, scalable and programmable IQPCs.

1.4.1 Si-based platforms

Historically, silicon-based platforms were the first to be investigated, and the most successful towards the implementation of IQPCs [127]. Such platforms include structures based on SiO_2 on Si, Si-on-insulator (SOI) and SiN on SiO_2. The very first demonstrations were conducted on silicon-on-silicon WGs, with the first implementation of linear optics based on chip quantum gates [128]. The large mode size typical for these structures enables simple coupling to fibers and free-space optics, which offers early opportunities for experiments with passive elements on the chip. Silica-on-silicon platforms are still being actively used [101, 103], but have been increasingly surpassed by SOI-IQPCs [166], which are better suited for processing quantum information on a large scale. They have several advantages over the other existing alternatives: they are transparent to photons at the telecommunications wavelengths, they have a strong nonlinearity of $\chi^{(3)}$, which enables compact single-photon source designs, and they benefit from the extensively developed manufacturing techniques in the field of silicon electronics and photonics and compatibility with the CMOS industry.

1.4.2 Single photon generation and integration

Integrated single-photon sources based on silicon chips typically rely on the spontaneous four-wave mixing (SFWM), a $\chi^{(3)}$ nonlinear process in which photon pairs are produced spontaneously from a pump beam, following energy conservation and phase-matching. SFWM sources have been implemented on silica-on-silicon [173], SOI [35], SiN-on-silica [92] platforms (see Fig. 1.11), in a variety of successful proof-of-principle photonic quantum inforation demonstrations. The Poissonian statistics of the nonlinear generation process, however, imposes a fundamental limit to the efficiency and scalability of these structures, as the pumping level, and thus the pair-generation rate, must be kept low in order to avoid multiphoton creation events. Time [71] and spatial [21] multiplexing techniques have been employed to improve source efficiency by up to 66.7 % [21]. It has been recently shown that an array of 18 SFWM single photon sources in SiO_2 WGs [173] can generate highly indistinguishable and highly pure

photons with a heralding efficiency of 50 %. In addition, the source can be used to generate entangled photons [46]. A silicon chip that embeds two sources, frequency demultiplexers and reconfigurable guided-wave optics can perform two-photon tomography or Bell CHSH tests on the chip [165]. Recently, high-dimensional entanglement generation has been achieved in a large-area Si chip with 16 SFWM sources [191], and coherent control over the generated states has also been demonstrated [80].

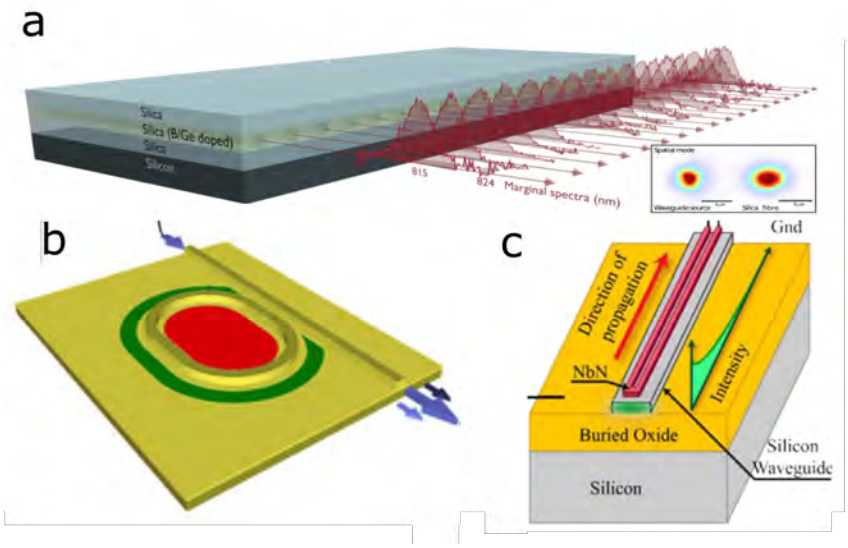

FIGURE 1.11 a) An array of heralded single-photon sources on a silica photonic chip [173][Reprinted with permission from Optica 4, 90-96 (2017), The Optical Society of America]. b) Photon pair generation in a Si microring resonator [35]. c) Design of the traveling wave SSPD: a sub-wavelength absorbing NbN nanowire is patterned atop a Si WG to detect single photons. [119]

1.4.3 Large scale integrated photonics

So far, the vast majority of integrated quantum-optical experiments have been based on WG systems that consist of N interferometer circuits that perform uniform transformations for N spatial modes. In 2001, Knill, Laflamme and Milburn showed in their groundbreaking work [78] that uniform transformations or logical operations can be carried out with linear optics and in particular beam splitters. In a subsequent work, Rieck et al. showed the any discrete, uniform operator could be realized experimentally. The setup can be made reprogrammable as desired by implementing reconfigurable Mach-Zehnder interferometers that act as reconfigurable beam splitters (RBS) [15, 54]. Fig. 1.12a shows such an electrically tunable Mach-Zehnder interferometer with two phase shifters.

The RBS is realized with two 50 % reflectivity beam splitters with adjustable

internal and external phase shifters and corresponds to the linear-optical Bogoliubov transformation:

$$\begin{pmatrix} e^{i\phi}sin(\theta) & e^{i\phi}cos(\theta) \\ cos(\theta) & -sin(\theta) \end{pmatrix}$$

where ϕ is the phase difference between the two outer arms of the Mach-Zehnder interferometer and θ is the phase difference between the two inner arms. Control of the phases enables any rotation in the U(2) group. The ability to generate arbitrary transformations for a large number of spatial modes is at the expense of complexity. For example, any U(20) transformation would require a total of 190 reflecting beam splitter (RBSs), each of which is phased and requires 380 electrical connections [15, 54].

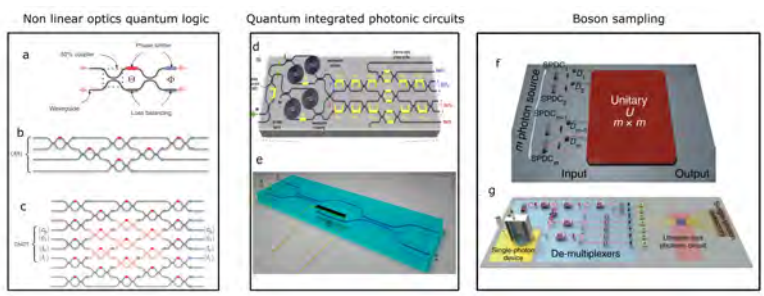

FIGURE 1.12 a) Reconfigurable beam splitter unit cell. b) Combination of several RBS cells for the implementation an arbitrary U(4) transformation c) Scheme of a CNOT gate. $|C_{0,1}\rangle$ and $|t_{0,1}\rangle$ are respectively the control and target qubit states [53]. d) Device integrating four-photon pair sources with a reconfigurable six-mode interferometer. It can generate on-chip entangled or separable states on-demand [147]. e) Scheme of an integrated tunable Mach-Zender interferometer. The phase difference is controlled by a bias driven heating resistance [42]. f) Schematic of the Boson Sampling algorithm [93]. g) Experimental setup for the boson sampling. Only the interferometer part is integrated. Single photon source (semiconductor QDs), demultiplexing setup, and detectors are off-chip. Reprinted with permission from [189].

1.4.3.1 Gate-based quantum information processing

The circuitry required for one of the most basic logic operations, called CNOT, is shown in Fig. 1.12c. This gate was implemented on chip in several silicon platforms [128, 22, 147]. With this technology, an on-chip demonstration of the factoring Shor's algorithm with two CNOT gates was realized [129]. The factorization of 15 was obtained with an accuracy of 99 %. The principle of the CNOT gate with linear optics requires the presence of ancilary waveguides which makes them intrinsically probabilistic. However, the demonstration of the CNOT operation with the detection of a photon on the auxiliary line can signal that the successfully processed qubits are available for use in the larger architecture. The first heralded CNOT gate was implemented on a SiO_2 chip that could also implement universal linear optical operations [15]. A similar

laser-written SiO_2 chip was used as the platform for integrated quantum teleportation with an average fidelity of 89 %. An outstanding capability of RBSs is the possibility of reprogramming a single chip, enabling it to process several quantum tasks and algorithms. In 2012, Shadbolt et al [164] reported on the first fully reconfigurable two-qubit quantum processor on a SiO_2 chip. The device consisted of two symmetrically designed entangled CNOT logic gates, which enabled the preparation, manipulation and processing of quantum states on the chip. The device could create any maximum and not maximum entangled states, perform thousands of different high-fidelity quantum experiments related to the violation of the Bell inequality and the calculation of ground state molecular energy [123]. Further work on other silicon platforms confirmed these possibilities [42, 131], in particular with the implementation of 98 different logic gates on the same programmable chip with an average fidelity of 93 %. Carolan et al. [15] recently proposed the first universal and fully reprogrammable linear-optic chip, and demonstrated its ability to perform several key applications, such as heralded quantum logics, entangling gates, boson sampling with verification tests and six-dimensional complex Hadamard operations. A later publication demonstrated the outstanding proficiency of the device by showing its ability to perform quantum simulation on several vibrational molecule processes [171]. A universal linear optical circuit has also recently been described in a silicon nitride-on-silicon platform [180].

1.4.3.2 Boson sampling

A direct and appealing application of the IQPC is boson sampling. Taking into account M indistinguishable photons that are injected into a linear optical circuit with N modes, the task of boson sampling is to take a sample from the probability distribution of single photon measurements at the output of the circuit [13].

Solving this problem in a classical computer entails the calculation of the permanent of the unitary matrix representing the linear optic circuit, a task that is computationally very demanding, of #P-complete complexity [191]. Indeed, it is believed that for a sufficiently large number of photons and optical channels, the problem may be more efficiently solvable in a photonic quantum simulator than by classical algorithms. Whereas this would constitute a first demonstration of quantum supremacy, the number of photons and channels required for such demonstrations is currently a moving target. Boson sampling does not require any ancillary line or entangling operation as in the Knill, Laflamme, and Milburn schemes [78]. While boson sampling is not universal, it can implement a classically difficult task with far fewer physical resources than a full linear optical quantum computer setup. The technical requirements are the implementation of efficient sources for single photons, linear interferometers and efficient single-photon detectors. As highlighted in the previous sections, these requirements are met by the various Si platforms. Therefore, shortly after the theory was published, several groups simultaneously reported on their experimental

implementation [182, 174, 13, 17]. They were all based on the injection of three photons into a five- or six-mode interferometer-on-chip circuit. Interestingly, the demonstrations with the highest number of photons are based on off-chip single semiconductor QD demultiplexed photons [91, 191, 189], see Fig. 1.12(g). Due to the probabilistic nature of SPDCs, the probability that the source generates simultaneously N photons decreases exponentially as N is increased. A variant called scattershot boson sampling [93], consisting of generating $M > N$ photons in order to increase the probability to effectively have a N photon input, has been proposed to make best use of the SPDC sources for boson sampling. The protocol was recently implemented with on-chip SFWM sources [117]. Another variant is the Gaussian boson sampling, which relies on an input of squeezed light [52] has been realized on the Si chip [117]. In contrast to the general-purpose computer, it is unlikely that boson sampling can be verified exactly by classic computers, especially since they are associated with the estimation of large matrix permanent elements, an unsolvable task for them. This posed the problem that no result of the boson sampling could be certified. However, various approaches were successfully implemented in the integrated optics, which made it possible to distinguish between uniform and boson scanning or between quantum and classic distribution.

1.4.4 III-V Semiconductor integrated optics

Another promising approach to realizing IQPCs is the use of III-V semiconductor materials. Unlike silicon, such materials feature a direct bandgap, allowing efficient light generation. Of particular relevance to quantum optics is that semiconductor quantum dots can be produced in III-V semiconductors, which can act as *deteministic* single-photon sources - as opposed to the spontaneous generation of parametric nonlinear processes such as SFWM. This is a considerable advantage over silicon: provided that the deterministically generated photons are efficiently collected into the WG circuits, the likelihood of success of on-chip logic operations is dramatically increased - a critical necessity for large-scale circuits. This also creates the possibility to implement scattershot Boson sampling.

GaAs is a well-known and mature material system with well-established manufacturing techniques and a long history of photonics integration, which offers many advantages for IQPCs. Its high refractive index enables high light confinement, and the creation of relatively low-loss waveguides. The large electro-optical effect in GaAs offers great opportunities for the routing and manipulation of photons. The integration of QDs in nanophotonic GaAs structures that aim at the deterministic generation of individual photons has achieved remarkable success in recent years. In addition, the implementation of on-chip detectors in GaAs WGs has attracted much community attention and paved the way for the first fully integrated semiconductor IQPCs.

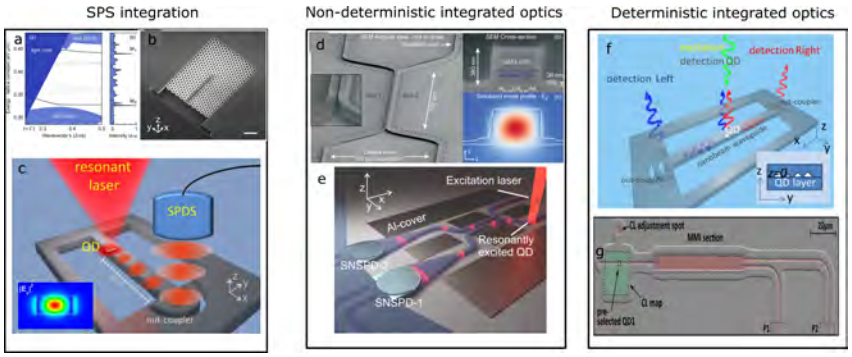

FIGURE 1.13 a) Calculated band structure for TE modes of an infinite PhC WG. b) Scanning electron microscopy picture of a PhC WG [159] c) Experimental scheme for the observation of resonance fluorescence QD coupled to a WG [97]. d) Scanning electron microscope image of a beam splitter evanescent field coupler implemented with ridge WGs [140]. e) Schematic representation of a fully integrated Hanbury Brown and Twiss experiment, comprising the SPS, the beam splitter and two integrated SNSPDs.[Reprinted with permission from [161]. Copyright (2018) American Chemical Society] f) Nanophotonic waveguide used for demonstration of chiral emission from an embedded quantum dot [20]. g) Integrated multimode interference beam splitter fabricated using in situ EBL technique[Reprinted with permission from [153], Copyright (2018) American Chemical Society]

1.4.5 On-chip single-photon generation

On-chip single-photon sources are realized using the radiative recombination from an excitonic state of a single QD [104]. QDs proved to be very efficient emitters of single photons and entangled photons [4]. They can be electrically driven [199], non-resonantly and resonantly addressed [108]. The generation of indistinguishable photons on demand requires a resonance laser that addresses the on-chip QD for better pump filtering. Efficient photon collection, low-loss waveguiding of light along the circuit and a good connection between the various functionalities are the main requirements for effective semiconductor IQPCs. The integration of QDs in WGs has proven to be particularly efficient. Photonic Crystal (PhC) [159, 82, 7], free-standing [97, 36] and ridge WGs [67, 61] are the two most popular approaches for on-chip collection and the transport of photons.

Photonic Crystal (PhC) WG structures have the advantage that they offer tight confinement and high coupling efficiencies between quantum emitters and propagating modes [83, 98, 133]. A popular type of PhC WG consists of a missing row of holes in a triangular lattice of holes ecthed into a semiconductor slab [94]. In such structures, the PhC photonic band gap provides strong lateral confinement for light, leading to the formation of guided modes with strong field concentration within the line-defect. Efficient coupling of quantum emitter radiation to such line-defect modes arises due to the strong field confinement. The coupling efficiency can be further improved if the emitter is, in addition, resonant with a WG slow-light mode, for which propagation velocity is much

lower, in comparison with regular modes [98]. Efficient routing in PhC WGs has been reported for 900 nm [82] and for photons with a telecommunications wavelength of 1300 nm [7] with efficiencies up to 98 % [94, 5]. PhC-WGs are also very practical for modifying the local density of states and allow manipulation of the emission direction and polarization (see section 1.4.6). The main obstacles to the implementation of all-PhC circuits are the typically high loss rates (of the order of dB/mm) [177] and the mechanical fragility of large, free-standing membrane PhC structures.

Free-standing channel WGs [97, 36] offer a comparable level of optical confinement and slightly better propagation losses than PhC WGs, with a less complex geometry. This class of WGs was used by Javadi *et al.* [36] to create an interface between a single photon and a QD spin with high spin preparation fidelity, and also a single-spin photonic switch. Like with free-standing membrane PhC WGs, the mechanical fragility of such structures creates challenges towards the creation of larger circuits.

Ridge WGs are an attractive alternative to both PhC and free-standing channel WGs, being mechanically robust, at least one order of magnitude less lossy, though offering a comparatively modest spatial confinement, nonetheless reasonable for light-matter interactions. Enhanced light-matter interaction can furthermore be enhanced though a compatible cavity, such as the Bragg grating cavity WG demonstrated by Hepp *et al.* [61]. The combination of PhC cavities connected to ridge WGs, a strategy that alleviates the mechanical fragility issue while preserving strong optical confinement for enhanced interaction with QDs, was demonstrated in ref. [40], using a one-step lithography process. Coupling efficiencies of 70 % [40] between ridge and PhC waveguides were achieved, which allowed single-photon count rates of 3.5 MHz, to be achieved, exceeding typical rates obtained for single QDs in bulk.

Overall, ridge WGs have been widely used for the fabrication of more complex structures and paved the way towards the first integrated quantum optics experiments in GaAs. The following section describe such developments. GaAs platforms are particularly well positioned for integrating monolithic circuits from beam splitters, interferometers, and detectors, which are required to implement KLM schemes or boson sampling protocols. The possibilities of GaAs structures were first demonstrated in 2014 [192] by characterizing an interferometric circuit, while the single-photon sources were outside the chip. The Mach-Zehnder interferometer (MZI) with two directional couplers and two electro-optical phase shifters showed classic interference visibility of up to 98 % and Hong-Ou-Mandel quantum interference visibility of up to 95 %. The relative phase control, evidenced by oscillations of the output count rates as a function of differential delay between the MZI arms, is a critical achievement because it is the key to fine-tuning the circuit and achieving universal linear computing in GaAs. The integration of quantum emitters in GaAs WG beam splitter systems has been demonstrated several times, with different designs such as rib-WGs [140] and ridge-WGs [67]. They showed successful integrated beam splitting with 50/50

directional couplers and multimode WGs. Another robust option is the production of multimode interference beam splitters, a technology that is already used in Si materials [122]. It was demonstrated with free-standing evanescent coupling beam splitters [130]. An important step forward in the production of practical semiconductor IQPCs was made with the implementation of a single-mode on-chip GaAs WG beam splitter. The device was addressed from above in an orthogonal configuration and the resulting laser filtering is very efficient since a multi-photon probability of only 0.18 was measured [160]. The development of the superconducting on-chip detectors in GaAs [139, 137] enabled the first demonstration of the fully integrated Hanbury Brown and Twiss experiment [161].

This series of advances has reached its technological limits due to the randomness of the manufacturing process related to the self-assembled expitaxial growth of the considered QDs. A very large number of devices must be manufactured and characterized before a single one can be selected for use. This represents a significant obstacle to the scalability of the semiconductor IQPCs. It is believed that deterministic manufacturing processes such as in-situ optical lithography [20] and in-situ EBL [47, 48] can overcome this problem, see section 1.3. As an example of recent progress in this direction, the integration of QDs into a 50/50 multimode interference beam-splitter has been mastered using in-situ EBL [153]. The fabrication technology offers the advantage of nanometer alignment accuracy and leads to IQPCs with maximized quantum optical properties. Thus, deterministic fabrication technologies open up realistic perspectives for the development of complex IQPCs with multiple monotonically integrated quantum emitters. As discussed in the next Section, deterministic fabrication methods are furthermore highly effective for the manipulation of the emitter's emission directionality inside a waveguide and potentially fulfill all the requirements for the complete implementation of on-chip logic quantum gates.

1.4.6 Chiral light-matter interaction

The WGs discussed above are powerful tools for exploring the interaction between light and matter. In most of these structures, light is confined transversely, in a plane orthogonal to the direction of propagation [90], and features a significant longitudinal electric field component. At specific, fixed locations (chiral points) within a WG, the electric field vector for a guided mode traveling in one direction rotates on the wafer plane. Locally, the field is circularly polarized, and carries a spin angular momentum. Inversion of the guided wave propagation direction leads to a sign change for the transverse spin component [90]. This means that chiral effects may be explored through the interaction of light with circularly polarized emitters. Specifically, a circularly polarized dipole located at a chiral point only emits guided waves that propagate in one direction, depending on the sense of rotation of the latter's electric field. The resulting emission chirality has been experimentally demonstrate with a variety of emitters and waveguides.

Fig. 1.14 shows examples of typical structures used to realize directional emission in GaAs quantum circuits.Fig. 1.14a shows the deterministically produced, free-standing orthogonal GaAs-WG structure, which is used to realize circular polarization directionality [96, 95]. This result was confirmed with another design based on a deterministic in-situ EBL approach [107] (Fig. 1.14b) where the lateral position of the emitter was controlled with nanometer accuracy to maximize in chiral interaction with propagating ridge-WG modes and to achieve maximum directionality contrast (Fig. 1.14c). In combination with an external magnetic field, the device enabled a high directionality contrast (90 %) of the circularly polarized emission. Directionality with high fidelity can be applied to the path-encoded qubit initialization and implemented directly in integrated quantum logic gates [168]. In the same publication, a scheme dealt with two additional beam-splitters and an additional WG for the device with two control target photons and three microwave pulses for initialization and manipulation of the QD state within a photonic crystal WG. Such capabilities are important steps towards the long-term goal of creating deterministic logic gate operation based on a single atom.

1.4.7 Diamond integrated quantum photonic systems

Diamond has emerged as a competitive platform for the development of reliable IQPCs thanks to new fabrication techniques [135]. It presents several advantageous structural and optical properties: a wide bandgap, high Debye temperature, high isotopic purity and low free electron concentration. NV centers feature long electron spin coherence times, on the order of microseconds. Single shot spin readout and coherent manipulation have been demonstrated [141]. This allowed for the generation of spin photon entanglement [183] and for the realization of loophole free tests of the Bell inequalities [60]. Silicon vacancy (SiV) centers can also be inserted in diamond and present a reliable alternative to NV centers. SiV centers present an interesting alternative with 90 % of its emission into the zero-phonon line, near–transform-limited optical linewidths and spin-lattice relaxation times approaching 1 minute as well as coherence times approaching 1 s [143]. Recently further emitters, such as Cr [2], Ni- [43], Ge- [192] and Xe- [65] emitters, attracted attention for their promising optical properties. Integrated circuits comprising color centers and optical cavities have been proposed as potentially deterministic platforms for generation and manipulation of quantum information [112].

1.4.8 Photonic Systems in Diamond Thin Films

Suspended diamond films or diamond structures placed on SiO_2 offer the high index contrast required for light confinement. Their development made full use of the techniques already established for the SOI platform. The first integration of multiple optical elements into a diamond film was demonstrated despite the

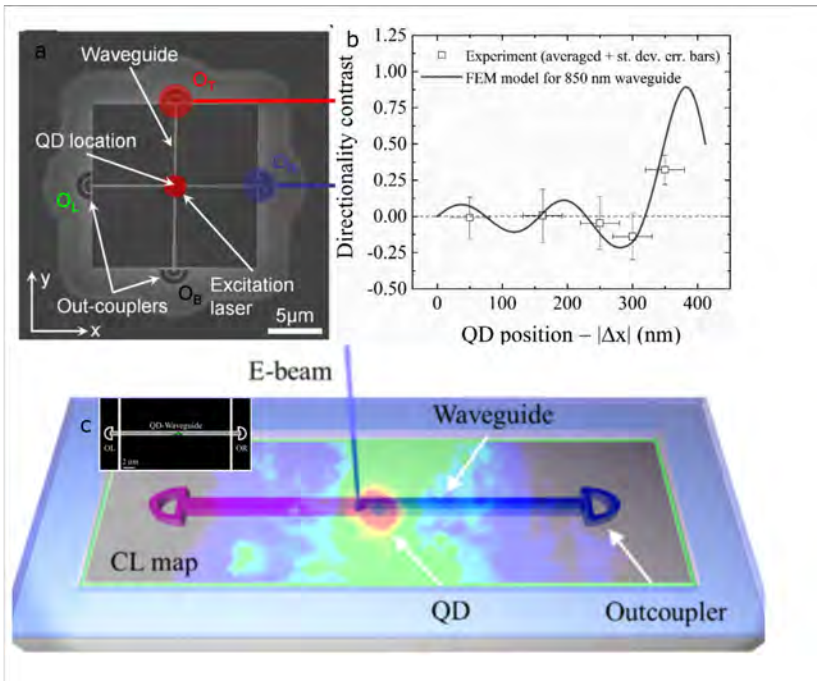

FIGURE 1.14 a) Spin-photon interface based on two orthogonal WGs where the polarization of the QD-emitted photon is converted into a path encoded photon [96]. b) Deterministically fabricated ridge WG as a chiral platform for QD photon emission. [Reprinted (adapted) with permission from [107], Copyright (2018) American Chemical Society]. On the two extremities, outcoupler gratings have been implemented for vertical efficient detection. c) Measured directionality of the photon emission as a function of the quantum dot position respective to the WG center [107]

difficulty in producing single crystal diamond films of uniform thickness. In 2011, Hausmann et al. [57] reported on the realization of a nanophotonic diamond that embeds a ring resonator with a high Q factor (Q = 12 600) that is evanescently coupled to a WG with grating couplers (Fig. 1.15 a). Here, single photons emitted by a NV center were coupled to the resonator mode and routed through the WG with a total extraction efficiency of 10 %. This result was reproduced in a very similar device with a remarkably strong improvement in the zero-phonon line in the resonator mode [39]. Another device, based on high quality single crystal diamond race track resonators and operating in the telecom C-band (1550 nm) associated with low loss diamond WGs terminated by polymer spot size converters, showed very high Q-factors (Q = 250 000) [56](Fig. 1.15 b)). An integrated optical thermal switch was fabricated with locally tuned WGs coupled to a resonator, reaching switching efficiencies up to 73 %. SNSPDs have been successfully implemented in polycrystalline diamond surface grown on silica-on-silicon substrate [134, 70].

1.4.9 Quantum photonic systems in bulk diamond

The first attempts to implement photonic circuits in diamond were carried out in bulk material, rather than thin films. Bulk diamond is preferred because color centers generally feature superior emission properties, in comparison to e.g., nanocrystals or thin films. The development of bulk diamond chips appears to have been dramatically slowed down by structural instabilities and complicated structuring techniques [62]. The main problem is the need for free-standing structures. However, the use of triangular ion etching enables the implementation of optical elements such as optical WGs, photonic crystals and cavities in bulk diamond. The recently developed laser writing technique in bulk diamond shows promising potential for the production of integrated photonic circuits [170]. There are still some challenges and difficulties, which will be discussed in more detail in section 1.6, before the first fully functional IQPC can emerge. However, the excellent optical properties of color centers motivate strong research in this direction and make them a potentially competitive solution for the future.

1.5 HETEROGENEOUS WAVEGUIDE SYSTEMS

Hybrid or heterogeneous integration allows the creation of photonic circuits composed of two or more different materials, each offering unique, usually complementary, optical properties. Such a "best of both worlds" approach in principle allows incorporation of desirable functionalities, provided by the different materials, to a single photonic chip.

Silicon-based photonic integrated circuits, for instance, are very promising for large system scaling, as foundry services offer the fabrication of user-designed, high quality integrated photonic circuits comprising thousands of elements on shared-project wafers [63]. Furthermore, optical losses in silicon

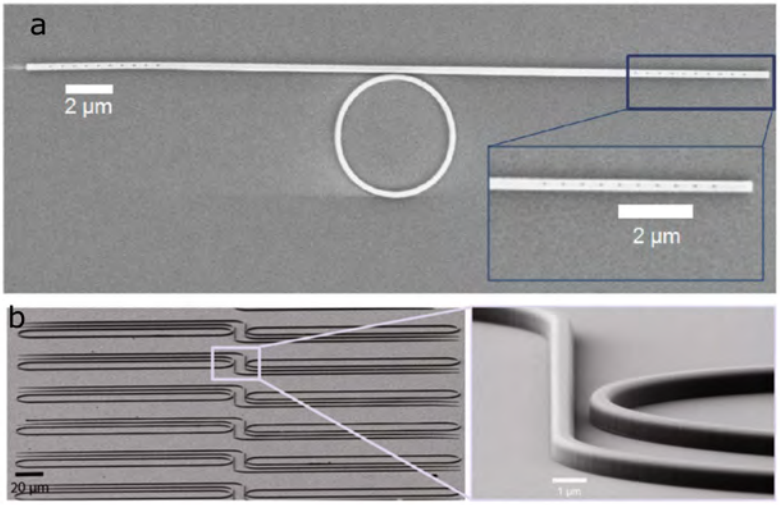

FIGURE 1.15 a) Diamond integrated nanophotonic network composed of a ring resonator evanescently coupled to a waveguide. [Reprinted (adapted) with permission from [57], Copyright (2012) American Chemical Society]. b) Single crystal diamond race-track resonators integrated with low-loss diamond waveguides terminated by polymer pads. [Reprinted (adapted) with permission from [56], Copyright (2013) American Chemical Society].

photonic WGs and related linear elements such as beam splitters, phase delays, linear filters, etc., can be made sufficiently low through design and process control, which allows large scale photonic circuits [16]. Thermal or carrier injection-based refractive index control, in addition, allows tunable phase delays, filters and modulators [79], which are important in both classical and quantum photonics. Lastly, silicon also offers pronounced Kerr nonlinearity, which, together with strong field confinement and dispersion control enabled by a high refractive index (≈ 3.5 for Si, ≈ 2 for SiN), allows efficient nonlinear optical processes [86]. Silicon's indirect bandgap, however, makes it an inefficient optical gain medium, imposing challenges for the creation of photonic circuits with elements such as on-chip electrically pumped tunable lasers, amplifiers and detectors.To circumvent this issue, heterogeneous integration processes started being developed in the mid-2000s, allowing introduction of direct-bandgap, III-V conpound semiconductors to silicon-on-insulator (SOI) wafers. Since the demonstration of the first silicon photonic laser with optical gain III-V semiconductor-based quantum wells [37], integration of other on-chip elements such as amplifiers, modulators, detectors, followed, with faster growth rate of devices per chip than homogeneous III-V devices [79]. Importantly, most of the early development of heterogeneous integrated photonic circuits has aimed at classical applications, primarily optical communications. Aiming at scalability, such development has been based on entirely top-down fabrication processes, starting from a bonded wafer stack.

As we show below, many such strategies have been applied towards quantum photonic circuits. The main focus of heterogeneous integration for quantum photonics has been the incorporation of single-photon sources and detectors onto otherwise passive, low-loss and (potentially) reconfigurable integrated photonic circuits. We next describe relevant efforts to date in these two directions, with considerable technical detail.

1.5.1 Heterogeneous quantum integrated photonic circuits with quantum emitters

The introduction of solid-state quantum emitters [3] onto otherwise purely passive integrated photonic circuits creates on-chip capabilities akin to those made possible through the introduction of III-V semiconductor-based optical gain media onto silicon photonics. Quantum emitters can act as high-rate, on-demand sources of indistinguishable single photons [169, 29, 88], providing the large on-chip photon fluxes necessary for a variety of quantum photonic systems. These include boson sampling type simulators [188, 91]. Emitters with optically addressable spins may furthermore act as stationary qubits in photonic networks, and, along similar lines, single-photon nonlinearities in single-emitter quantum cavity-electrodynamic systems [66, 178] may allow networks of deterministic quantum logic gates to be implemented.

A number of types of quantum emitters have been integrated onto photonic circuits to date, primarily using the techniques described in Section 1.3. We next describe some of the most relevant work demonstrated to date.

The work of Mouradian et al. [106] demonstrated integration of a SiN photonic circuit with long-lived quantum memories based on NVs in diamond, as shown in Fig. 1.16(a). The diamond quantum nodes consisted of micron-length WGs of $\approx$ 200 nm$\times$200 nm cross-section, bridging two low-loss SiN WGs over an air gap. Photonic design was such that 86 % of the NV zero phonon line fluorescence intensity at 638 nm would be launched into the diamond WG, in both directions, for an optimally positioned NV center. The diamond WGs also featured adiabatic mode transformers at the ends, consisting of linear width tapers down to 100 nm over 4 μm in length, for highly efficient (96 %) light transfer into SiN WG. The pick-and-place method utilized to experimentally produce the photonic circuits allowed separate fabrication and pre-characterization of the diamond WGs separately from the SiN WGs, and ultimately the deterministic integration of diamond WGs containing single, stable, negatively charged NVs onto the circuit. Experimentally, the fabricated devices were investigated at room temperature by confocally exciting single NV devices from the top with a 532 nm pump laser, and collecting the fluorescence both through the objective and through the SiN WGs, using a lensed single-mode fiber. The objective-collected signal showed second-order autocorrelation with $g^{(2)}(0)$ as low as 0.07,indicating good isolation between the NV and other fluorescence sources in the diamond WG. Cross-correlation between the fiber- and objective-collected signals on the other

hand yielded $g^{(2)}(0) \approx 0.48$, however, indicating the presence of considerable background emission, which was attributed to fluorescence due to scattering of the excitation laser into the SiN WGs. Nonetheless, an estimated flux of 1.45×10^6 NV-emitted photons/s was collected into one direction of the single-mode SiN WG. Cryogenic photoluminescence excitation (PLE) measurements at 18 K revealed NV zero-phonon linewidths of < 393 MHz, approximately 30 times wider than the natural linewidth for the $m_s = 0$ transition in bulk diamond. The broadened spectrum was at least partially due to spectral diffusion of the NV emitter, which was faster than the experimental integration times. Through a Hahn-echo experiment, an electron spin coherence time of $T_2 \approx 120\ \mu s$ was measured, which was comparable to that observed in the bulk diamond used to produce the WGs. To circumvent the issue of qubit inhomogeneities in the path towards large-scale quantum photonic integration, work by Wan *et al.* demonstrated the pick-and-place of arrays of diamond nano-WGs onto an AlN photonic circuit, as shown in Fig. 1.16(b) [187]. The process allowed inclusion of a 72-channel array of germanium-vacancy (GeV) and silicon-vacancy (SiV) centers embedded in the nanodiamond WGs. Photoluminescence spectroscopy at below 4 K temperatures revealed close to lifetime-limited emission linewidths for the two types of color centers. Strain-based tuning of the emission wavelengths was also demonstrated, via electrostatic actuation of the suspended nano-WGs. Although the demonstration in this work only involved single-photon launching into the AlN, the material offers a number of desirable optical properties, such as $\chi^{(2)}$ nonlinearities, as well as electro-optic and piezoelectric properties that can be used to create a number of on-chip functional elements [198].

The first report of hybrid integration of epitaxial QD-based single-photon sources on a low-loss silicon-based photonic circuit was by Murray *et al.* [109]. In this work, a bare strip of a GaAs wafer containing InAs QDs was orthogonally bonded to the cleaved facet of a Silicon Oxynitride (SiON) WG-based Mach-Zehnder interferometer (MZI), as shown in Fig. 1.17(a). Coupling of QD single-photons into one of the MZI input WGs relied on the chance spatial alignment of an individual dot to the latter; without a proper GaAs geometry to help funnel QD emission into the input WG, a theoretical maximum collection efficiency of about 3 % was predicted. The MZI featured integrated, nickel-chromium alloy heaters that allowed tuning of its coupling ratio, from ≈ 50 % to ≈ 100 % upon application of voltages up to 20 V. Operating at 4 K, the MZI was used as a splitter in a Hanbury Brown and Twiss (HBT) measurement, yielding $g^{(2)}(0) \approx 0.09$. In a later publication [31], the same group combined an array of tuneable InGaAs/GaAs QD single photon sources with the SiON WG circuit. The same bonding approach as in [109] was used here, though the QD wafer featured a regular array of emitters, with defined electric contacts, at a compatible spacing with the SiON WGs (Fig. 1.17(b)). The QDs were embedded in a diode heterostructure comprised of a weak planar cavity with 4 and 10 pairs of GaAs/AlGaAs distributed Bragg reflectors above and below a $\lambda/2$ spacer. A coupling efficiency of ≈ 8 % into the SiON was predicted for such source,

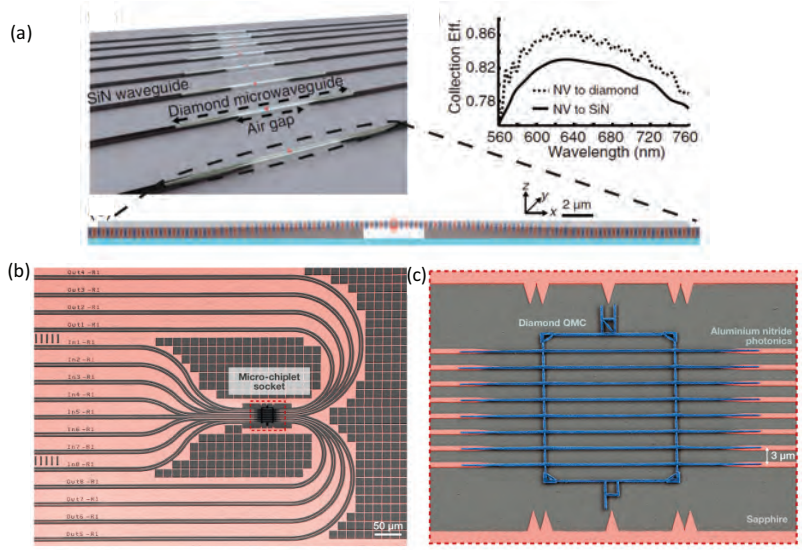

FIGURE 1.16 (a) SiN photonic circuit with integrated diamond WGs containing NV centers, from Mouradian *et al.* [106]. The simulated electric field produce by a single NV center at the WG center can be seen at the bottom of the figure, showing efficient light coupling to the SiN WG. Top right inset: dipole coupling efficiency spectrum into the diamond and SiN WGs. *(Reprinted from ref. [106] with permission from the American Physical Society.)*(b) AlN photonic circuit for large-scale diamond WG coupling, from Wan *et al.*. [187]. The micro-chiplet socket indicated at the center receives the diamond WG array chiplet in (c), via a pick-and-place approach. *(Reprinted from ref. [187] with permission.)*

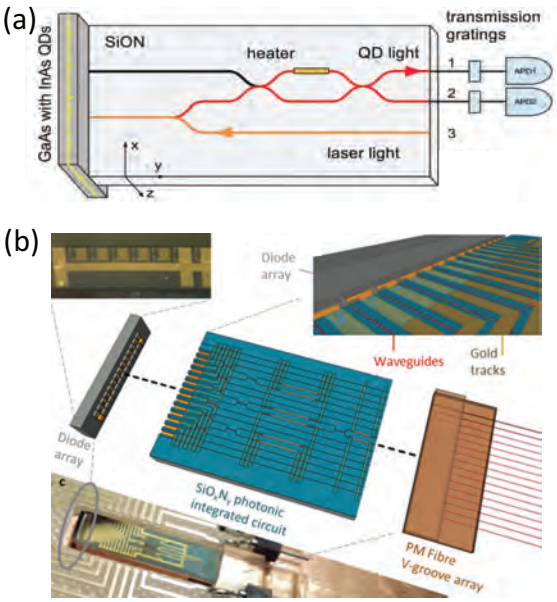

FIGURE 1.17 (a) SiON photonic circuit with side-bonded GaAs wafer containing InAs QDs, from Murray *et al.* [109]. The QDs here were in bulk GaAs. *(Reprinted from ref. [109] with permission from the American Institute of Physics.)* (b) SiON photonic circuit with side-bonded GaAs wafer containing InAs QD single-photon sources based on planar microcavities, from Ellis *et al.* [31]. The low-loss SiON photonic circuit was used to demonstrate interference of photons produced by two independent QD sources. *(Reprinted from ref. [31] with permission from the American Institute of Physics.)*

and spectral tunability was enabled through the DC Stark effect. Each WG in the SiON circuit could be addressed by a separate, electrically controlled QD-containing diode. Emission from neighboring diodes were independently tuned to degeneracy, and allowed observation of Hong-Ou-Mandel (HOM)-type interference with a visibility of $\approx$ 80 %, limited by source purity. The authors also used electrically-pumped wetting layer light, guided by the planar cavity, to pump individual QDs in separate diodes, demonstrating the possibility of an on-chip pump for single-photon emission.

In the work by Zadeh *et al.*, the pick-and-place technique was used to produce hybrid devices as shown in Fig. 1.18(a), composed of InP nanowires (NW) containing single InAsP QDs embedded in SiN WGs [200]. The high index contrast between the InP and SiN helped promote high collection efficiency for QD-emitted photons into a confined InP WG mode, and a slight tapering of the NW tip, with geometry controllable through growth parameters, allowed efficient launch of dot emitted photons into the SiN WG, with a theoretical maximum of 36 %. The III-V nanowire and QD were grown by a selective-area and vapor-liquid-solid epitaxy process. These microns-long, $\approx$ 100 nm diameter wurtzite

nanocrystals were plucked from the growth substrate using a tungsten tip mounted on a 3-axis movable stage, and transferred to a silicon chip, with <500 nm positioning precision. The receiving chip consisted of a Si wafer covered by a 2.4 μm SiO_2 film, which served as a low-index substrate layer, and featured prefabricated markers used to align the photonic circuits with respect to the nanowires. The sample was covered in SiN grown by plasma-enhanced chemical deposition (PECVD), and lithography and etching of the SiN were used to define the photonic circuits. The work in [200] showed coupling of single-photons from the InAsP QDs into a low-loss ($\approx$ 2.5 dB/cm at 880 nm) SiN WGs with an efficiency $\approx$ 24 %. The single-photon nature of the emission was verified through an HBT measurement of the QD photoluminescence signal under non-resonant excitation, collected from the WG facet, and showed multi-photon probability $g^{(2)}(0) \approx 0.07$. Importantly, the QD emission linewidth was of approximately 3.65 GHz. While this first demonstration was mostly concerned with outcoupling single-photons into the low-loss SiN WG, Elshaari *et al.* [34] later used the same basic platform to demonstrate filtering and multiplexing of single QD emission by on-chip SiN microring resonator-based add-drop filters, as shown in Fig. 1.18(b). The SiN add-drop filters, designed for critical coupling to SiN bus WGs, had a free spectral range (FSR) $\approx$ 0.96 nm with full width at half maximum (FWHM) of $\approx$ 0.13 nm at the QD emission wavelength, and incorporated metal microheaters which allowed thermo-optic wavelength tuning. The ring resonator's PMMA top cladding displayed a pronounced negative thermo-optic coefficient, $\approx 10\times$ that of SiN, which allowed tuning of the whispering-gallery modes by 120 % of the FSR with $\approx$ 15 V applied to the electrode heaters, and covering $\approx$ 40 nm of QD spectral range. Importantly, the photonic circuit design sought to minimize the thermal coupling between the filter electrodes and the QDs, the emission of which red-shifted slightly due to thermal coupling. Nonetheless, the tunable filter was used to drop one of the QD's trion emission line into an output WG, eliminating both the QD's exciton line and the nonresonant, 532 nm wavelength pump from the original WG-coupled signal, with suppression of $\approx$ 95 dB. The resulting $g^{(2)}(0) \approx 0.4$ for the dropped trion line demonstrated the effectiveness of the ring resonator as an on-chip spectral filter. A similar add-drop structure was also used to multiplex emission from two spectrally distinct QD sources placed at two of the microring inputs, as shown in Fig. 1.18(b). In Ref. [32], the same group demonstrated a SiN photonic circuit on piezoelectric magnesium niobate–lead titanate (PMN–PT) substrate, and used their microprobe-based pick-and place technique to incorporate QD nanowire single-photon sources. The piezoelectric substrate allowed voltage-controlled, mechanical strain-based spectral tuning of the QD emission, with a tuning rate of as much as 1.33 pm/V, as well as tuning of a microring resonator filter by a compatible rate of 0.96 pm/V.

In the work by Kim et al. [76], pick-and-place was performed with a focused ion beam (FIB) machine, yielding hybrid devices that consisted of an InP nanobeam containing InAs QDs (emitting in the 1300 nm telecom band), on top of Silicon-on-insulator (SOI) photonic WGs. In contrast with the nanowire-based

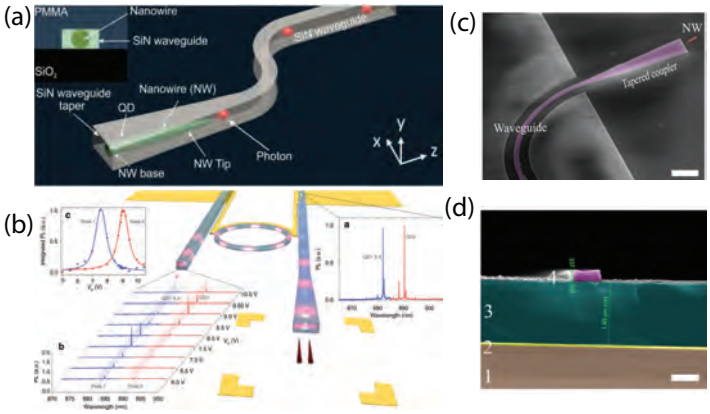

FIGURE 1.18 (a) Hybrid SiN WG with InP-based nanowire / QD-based single-photon source from Zadeh *et al.* [200]. *(Reprinted from ref. [200] with permission from the American Chemical Society.)* (b) Schematic of SiN microring resonator add-drop filter implemented work by Elshaari *et al.* [34], which incorporated nanowire / QD single-photon sources as in (a). Two single-photon sources, with different spectral characteristics, are pictured, coupling into the microring resonator via a bus WG on the right-hand side. The microring drops signals resonant with its whispering-gallery modes into a bus WG. Microheaters, depicted in yellow, allow the microring add-drop filter to be spectrally tuned. *(Reprinted from ref. [32] with permission from the Springer Nature.)* (c) Scanning electron micrograph of SiN WG and InP nanowire (NW) single-photon source, from the work of Elshaari *et al.* [32], where NW emission could be tuned via strain induced from the magnesium niobate–lead titanate (PMN–PT) substrate on which the circuit was produced. (d) False-color SEM of the cross section of the SiN WG in (c). Regions labeled 1,2,3 and 4 are the piezoelectric PMN-PT substrate, gold electrode, silicon oxide substrate and silicon nitride WG respectively. *(Reprinted from ref. [32] with permission from the American Chemical Society.)*

platform of Zadeh et al. and Elshaari *et al.* [200, 34], QD-containing nanobeam geometries were produced through lithography and etching steps. This allowed the creation of a photonic crystal back-reflector on the nanobeam, consisting of a periodic array of ≈100 nm diameter etched holes, which was used to direct the QD emission to one direction. Lithography also allowed the creation of mode transformers at the end of the nanobeam, for efficient power transfer into the silicon WG. An outcoupling efficiency of ≈ 32 % was theoretically predicted into the Si WG, for an ideally positioned QD. The theoretical efficiency breakdown was 71 % of QD emission into the nanobeam's fundamental TE guided mode, and coupling efficiency of 45 % from such guided mode to the silicon WG, through an adiabatic mode transformer. An on-chip silicon photonic 50:50 beamsplitter was implemented, which directed photoluminescence from a single QD between to WGs that were terminated into two free-space grating outcouplers. Emission lines from the same QD could be seen in light collected from the two grating couplers, and an HBT measurent revealed $g^{(2)} \approx 0.25$ for one of the lines, proving single-photon emission. In a more recent development, using the same FIB microprobe-based pick-and-place technique, the same group integrated InP nano-WGs containing InAs QDs onto $LiNbO_3$ WGs [1], and demonstrated HBT single-photon correlation measurements with an on-chip beamsplitter and off-chip detection. Although the electro-optic and nonlinear optical properties of $LiNbO_3$ were not explored, this work showed that efficient coupling of QD emission into $LiNbO_3$ materials is possible, which creates many opportunities for fast on-chip single-photon switching and wavepacket manipulation [132].

In the work by Katsumi *et al.*, InAs QD-containing GaAs nanobeam photonic crystal cavities evanescently coupled to underlying GaAs WGs were produced through a transfer-printing process [72]. Here, a Polydimethylsiloxane (PDMS) stamp was used to lift suspended GaAs nanobeams from a processed GaAs wafer. The destination substrate consisted of GaAs-on-SiO_2 wafer onto which GaAs ridge WGs were etched, covered by a spin-on-glass (SOG) top cladding. The small mode volume (≈ 0.5 cubic wavelengths) of the designed nanobeam photonic crystal cavity's fundamental mode allows ≈ 99 % quantum dot coupling to the latter, primarily through Purcell radiative rate enhancement, even for loaded quality factors Q in the few thousands. Importantly, Q is dictated by the coupling rate between the cavity and the WG, which is determined by the vertical distance d between the two. Although the coupling efficiency into the WG can be limited by parasitic losses to radiative modes as the distance d between guide and cavity goes below a certain point, efficiencies in excess of 99 % are still achievable theoretically. Experimentally, the estimated emitter–cavity coupling efficiency was $\beta \approx 87$ %, the cavity-WG coupling efficiency was $\eta \approx 72$ %, for a total single-photon launch efficiency of 63 % into the GaAs WG. Similar performance was also predicted for Si_3N_4 and Si WGs (in fact, integration of GaAs/InAs QD single-photon sources onto glass-clad silicon photonic WG processed by a CMOS foundry was demonstrated in [74], shown in Fig. 1.19). More recently, the same technique was used to demonstrate thermally-tunable

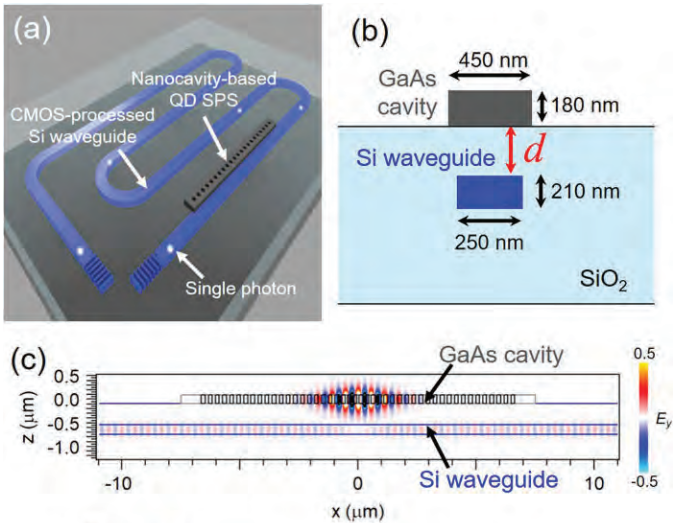

FIGURE 1.19 CMOS-based integrated photonic circuit with on-chip single-photon sources (SPS) based on GaAs nanobeam photonic crystal cavities containing InGaAs QDs (QDs), from Katsumi *et al.* [74]. (a) Artistic rendering of Si photonic WG with evanescently coupled GaAs photonic crystal nanobeam. (b) Cross-section of the circuit in (a), at the nanocavity position. (c) Simulated electric field of photonic crystal cavity mode, showing evanescent coupling to the underlying Si WG. *(Reprinted from ref. [74] with permission from the American Institute of Physics.)*

QD single-photon sources on CMOS silicon photonic circuits, implemented by adding a thermal heating pad to the GaAs device [73]. Independent QD spectral tuning of up to $\approx$ 1 nm was demonstrated, though corresponding to an effective temperature swing of $\approx$ 15 K. This capability nonetheless allowed in-situ wavelength matching between two dissimilar QD sources integrated on the same silicon chip. Multiplexing of the QD source signals in an on-chip 2×2, multimode interference coupler based 50:50 splitter was also demonstrated, though two-photon interference effects were not observed. In work by Osada *et al.*, the same group also demonstrated strongly coupled cavity QED systems based on single InAs QDs in GaAs photonic crystal cavities on a CMOS silicon photonic chip [115].

The work by Davanco *et al.*, showed that direct wafer bonding could be leveraged to produce Si_3N_4 WG-based photonic circuits incorporating single QDs as single-photon sources [23]. In this work, a heterogeneous GaAs/Si_3N_4 stack was produced with a low temperature, oxygen plasma-activated wafer bonding procedure [37]. The stack consisted of a silicon substrate covered by 3 μm of thermal SiO_2, 550 nm of stoichiometric Si_3N_4 produced through low-pressure chemical vapor deposition (LPCVD), and an approximately 200 nm thick layer of GaAs containing InAs QDs at half thickness. After wafer bonding, fabrication proceeded through two subsequent, aligned electron-beam lithography and etch-

ing steps, and could produce circuits as shown schematically in Fig. 1.20(a). In these devices, compact GaAs nanophotonic structures hosted single InAs QDs, and were designed to launch emitted photons efficiently into the Si_3N_4 WGs composing the photonic circuit. The GaAs nanophotonic structure comprised a photon capture WG and a mode transformer, both with nanometer-scale features defined by electron-beam lithography. The photon capture allowed efficient coupling of emitted photons into the fundamental transverse-electric (TE) GaAs ridge mode in Fig. 1.20(b). The mode transformer converted the fundamental TE GaAs ride mode into the fundamental TE Si_3N_4 ridge mode shown in Fig. 1.20(d). As indicated in Figs. 1.20(a)-(c), the mode transformer consisted of an adiabatic width taper for both the GaAs and Si_3N_4 ridges. A number of nanometer-scale resolution geometries were generated in the GaAs layer, such as nano-WGs (Fig. 1.20(a)), WG-coupled microring resonators, (Fig. 1.20(b), all of which were efficiently coupled to the underlying Si_3N_4 WGs via adiabatic mode transformers, as indicated in Fig. 1.20(a). Although the III-V material contained a high density of randomly-positioned QDs (> 100 μm^2), single-photon emission from single QDs coupled to nano-WGs and microring resonators were observed, by pumping the QDs in the p-shell with a tunable laser. For these devices, the QD single-photon emission (with raw $g^{(2)}(0) < 0.4$ overall) was launched, with > 90 % efficiency, into the Si_3N_4 WG,via the adiabatic mode transformers. A further, relevant detail is that the emitted single photon streams were collected from the Si_3N_4 WG facets with a lensed optical fiber in endfire configuration, as typically done for testing classical integrated photonic devices. The fiber-to-Si_3N_4 coupling efficiency was ≈ 20 %, which, while also typical of integrated photonic devices, can potentially be significantly improved by proper Si_3N_4 mode transformer design design. Regarding β-factors, the nano-WG were designed to feature $\beta = 0.35$ for the fundamental transverse-electric (TE) GaAs-ridge mode in one direction, and for a QD with transverse dipole moment at the center of the GaAs ridge, even though the structure was not fully optimized (a design with $\beta > 0.45$ is provided in the publication). For a single dot in a representative, fabricated GaAs nano-WG, $\beta \approx 0.20$ was estimated - a value that is not too far from the theoretical maximum. It is worth noting that the QDs were not deterministically positioned in the nano-WG in this case, and so both positions and dipole moment orientations were likely sub-optimal. Lifetimes observed in nano-WGs were of $\approx$1.5 ns, close to the expected value for an InAs QD in bulk. No radiative rate enhancement was expected here, as nano-WGs are non-resonant. In contrast, in microring resonators, weak-coupling of single dots to whispering-gallery modes of quality factors in the 10^3 to 10^4 range led to significantly reduced radiative lifetimes, with an estimated Purcell factor $F_p \approx 4$. This value was not too far from the theoretically predicted based on the microring Q-factor and mode volume $V_{\text{eff}} \approx 75(\lambda/n)^3$. This work extended the application space of a mature, scalable, top-down heterogeneous photonic integrated circuit platform into the quantum realm. The technique is unique in allowing independent, flexible, and nanometer-scale resolution tailoring of

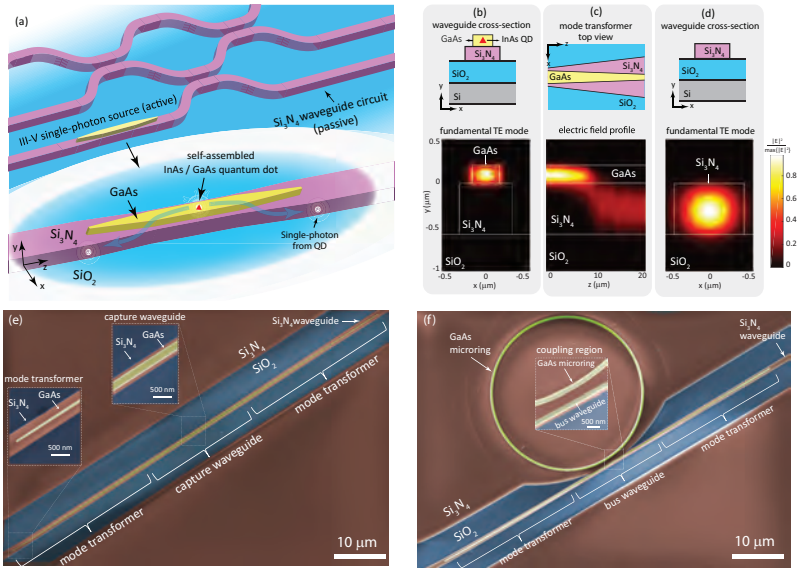

FIGURE 1.20 Wafer-bonding based heterogeneous Si_3N_4 photonic circuits with single-photon sources based on InAs QDs in GaAs nanophotonic geometries, from Davanco *et al.* [23]. (a) Idealized Si_3N_4 photonic circuit showing passive WGs in pink and local III-V semiconductor-based single-photon sources. The source depicted comprises a GaAs ridge WG on top of a Si_3N_4, with cross-section as shown in (b), top. The GaAs ridge contains a single QD, which emits single-photons into the the transverse-electric (TE) mode in the bottom panel of (b), with high efficiency. (c) Top: Adiabatic mode transformer, implemented through linear width tapers for both GaAs and Si_3N_4 ridges, allows efficient transfer of emitted QD light from the mode in (b) to the Si_3N_4 mode in (d). (e) False-colour scanning electron micrograph of a fabricated nano-WG with mode transformers, as depicted in (a). The insets show details of the photon capture and mode transformer sections of the device. (f) False-colour scanning electron micrograph of a fabricated, hybrid microring resonator evanescently coupled to a bus WG. The WG has mode transformers that allow the access to the Si_3N_4 WG. *(Reprinted from ref. [23] with permission from Springer Nature.)*

both active and passive photonic circuit elements with precise and repeatable, sub-50 nm alignment defined strictly by lithography.The underlying Si_3N_4 WGs demonstrated here provide not only a low-loss medium for single-photon propagation on-chip, but also the possibility of using nonlinear optical processes for functionality. An example is four-wave-mixing-based quantum frequency conversion, which has been demonstrated in Si_3N_4 microring resonators [86, 167] made out of WGs with comparable dimensions and the same materials as in ref. [23]. The introduction of elements such as on-chip delay lines, high quality Si_3N_4-based filters, and microring add-drops, can also be envisioned, as well as integration with WG-based superconducting single-photon nanowire detectors [120]. Finally, the fabrication process can be adapted for materials such as AlN and $LiNbO_3$, which may enable active electro-optic phase control.

While the work from ref. [23] featured devices with randomly positioned

QDs, in ref. [156] heterogeneous nano-WGs containing precisely positioned single QDs were deterministically produced via the in-situ EBL technique of refs. [51, 48, 152, 107], see Sec. 1.3. To fabricate the devices, single QDs were initially located through cathodoluminescence spectroscopy and imaging, on a heterogeneous bonded wafer. Immediately after localization, proximity-corrected gray scale in situ EBL was performed at 7 K with unchanged beam column settings to define the GaAs WG taper patterns and alignment marker for the Si_3N_4 layer, both aligned to the identified QDs. The Si_3N_4 WG patterns were defined as in ref. [23], using the GaAs alignment markers. An important result of this work was that, for a QD located sufficiently far from the GaAs etched sidewalls, post-selection indistinguishable single-photon emission could be observed. The QD here was located in the middle of a $\approx$ 800 nm GaAs ridge, and was pumped in the p-shell. High-resolution spectra of one of the QD's emission lines (likely a trion) revealed a Voigt lineshape with a linewidth of $\approx$ 2.2 GHz full width at half-maximum (FWHM). The Lorentzian component of $\approx$ 1 GHz FWHM suggested homogeneous broadening beyond the Fourier limit of $\approx$0.1 GHz, likely due to dephasing from phonon interactions. The Gaussian component, with a linewidth of approximately 1.5 GHz FWHM suggested inhomogeneous linewidth broadening due to spectral diffusion. A Hong-Ou-Mandel (HOM) measurement of the single-photon stream revealed clear evidence of two-photon interference with a visibility of approximately 89 %, and a coherence time of approximately 300 ps. The coherence time here indicates a postselection time window where indistinguishable photons are available. Precise alignment of the EBL patterns with respect to the QDs is essential to avoid excessive proximity to etched sidewalls, which may lead to degradation of quantum efficiency and, especially, coherence [87]. The observation of a 2.2 GHz linewidth from a positioned QD emission line, and subsequent demonstration of two-photon interference, suggested that the required precision can be met in a heterogeneous integration platform, via the positioning method described above.

Monolayer transition metal dichalcogenides and (TMDCs) and monolayer and multilayer hexagonal boron nitride (hBN) have been shown to support spatially localized single photon emitters, producing light at visible and near-infrared wavelengths. Peyskens *et al.* has demonstrated integration of monolayer WSe_2 single-photon emitters with SiN WGs [124]. The monolayer WSe_2 here was produced though an exfoliation process, and the transfer onto the SiN WG led to formation of localized emitters at stress points at the top edges of the SiN ridge. The emitter launched single-photons into the SiN, as verified by HBT measurements. The maximum theoretical single-photon coupling efficiency was $\approx$ 8 %, relatively low due to a lack of an optimized photonic structure to capture and launch photons into the WG. A strategy to improve this efficiency through cavity coupling is discussed in the publication. Single emitters based on WSe_2 monolayers were also integrated onto a Titanium in-diffused lithium niobate directional coupler in work by White *et al.* [196], however very low single-photon collections efficiencies ($\approx$ 0.1 %) prevented observation of the HBT effect.

The work of Khasminskaya *et al.*, demonstrated a nanoscale, electrically driven single-photon emitter using WG-coupled semiconducting single-walled carbon nanotubes (sc-SWCNTs), coupled to a silicon photonic circuit [75]. The circuit consisted of a Si_3N_4 WG hosting, at its center, a CNT that was contacted by gold electrodes, for carrier injection. The circuit also featured niobium nitride (NbN) superconducting nanowire single-photon detectors (SNSPDs) defined on top and at the two ends of the Si_3N_4 WG. The SNSPD detectors comprised a single meander with 80 nm width and 100 nm gap size, and a critical temperature $T_c = 10.7$ K. Interestingly, because the nanotube emitter was located at the center of the WG, emission towards the two detectors at the WG ends was equally likely, so the entire configuration was equivalent to an HBT setup. Generation of single-photons from sc-SWCNTs was postulated to take place via radiative recombination of defect-localized excitons, after carrier injection through a Schottky contact. At 1.6 K, the nanotube's electroluminescence spectrum revealed a peak around 1370 nm, with a FWHM of ≈ 30 nm. Running the HBT measurement at various injection current levels yielded anti-bunching curves that indicated non-classical light generation from the nanotube. Anti-bunching with $g^{(2)}(0) < 0.5$ was observed (within experimental noise) only for the lowest current injection level, though increased currents led to decreased levels of single-photon purity.

1.5.2 Heterogeneous quantum integrated photonic circuits with single-photon detectors

Detector integration is one of the necessary building blocks on the way to a fully integrated device. On-chip detection enables single-photon counting correlations and photon-number resolving measurements directly on chip, alongside single-photon generation. In addition, it allows one to avoid the significant photonic losses, electronic delays and wiring complexity involved in off-chip detection. Superconducting nanowire single-photon detectors (SNSPDs) have been extensively explored in quantum integrated photonic circuits. With quantum efficiencies of over 90 %, response times in the picosecond regime, negligible dark counts, detection rates of over 100 MHz over a broad spectral range, and potential for photon-number resolution [45], SNSPDs are highly attractive for quantum photonics, however require cryogenic temperature operation. Single-photon detection by an SNSPDs is based on the formation of a transient resistive barrier across an initially superconducting wire following absorption of a single photon, which produces a measurable voltage pulse. The resistive barrier is formed by breaking of Cooper-pairs by the incident photon, which leads to formation of a hotspot across the wire. Superconductivity is later restored after healing of the hotspot, in time scales of typically tens of picoseconds. Critical for high performance SNSPD operation are the quality of the superconducting material film, as well as nanowire geometry and imperfections. The former consideration is associated with deposition methods as well as substrate quality,

and the latter with high-resolution lithography and etching process quality. Both considerations are additional challenges in the creation of waveguide-integrated detectors. The work discussed below covers significant efforts to date towards SNSPD integration within integrated photonic circuits.

In 2011, Sprenger *et al.* [172] demonstrated NbN SNSPDs integrated onto GaAs ridge waveguides, following the same working principle as non-waveguided, superconducting nanowire detectors demonstrated up to that point. The detectors were deposited and patterned on top of GaAs ridge waveguides, and sensed the evanescent tail of the modal field on the surface. A detection efficiency of approximately 20 % telecom wavelengths was reported, with response time in the nanosecond range, and a timing accuracy of approximately 60 ps, all at <4 K operating temperatures.

Around the same time, Pernice *et al.* demonstrated traveling wave niobium nitride (NbN) SNSPDs atop silicon nanophotonic WGs on a circuit [120], and have shown that such integration can lead to drastic increase of the absorption length for guided photons, as compared to normal incidence. An on-chip single-photon detection efficiency up to 91 % at telecom wavelengths was achieved. Dark counts in the Hz range were achieved without compromising the efficiency, as well as a timing jitter of 18 ps. The high temporal resolution allowed observation of ballistic photon transport in silicon ring resonators produced on the same chip as the detectors.

In work by Schuck *et al.* [158] sputter-deposited NbTiN SNSPDs were produced onto a Si_3N_4 photonic circuit, shown in Fig. 1.21(a), that formed part of a Hong-Ou-Mandel (HOM) setup, featuring a directional coupler to combine incoming photons and route them towards two on-chip detectors. An on-chip detection efficiency of 11.5 % and a typical dark count rate in the Hz range when biasing two detectors close to the critical current were achieved for operation at 1.7 K. These characteristics allowed the observation of two-photon interference with a visibility of 97 % from an off-chip spontaneous parametric down-conversion photon-pair source.

Reithmeier *et al.* [139] demonstrated integration of NbN SNSPDs on top of GaAs-on-AlGaAs WGs containing InAs QDs as shown in Fig. 1.21(b), with a detection efficiency of ≈ 0.1 %, and a timing jitter of 72 ps. The low efficiency here was associated with the 10 nm NbN thickness. Nonetheless, in later work, a similar type of device was used to perform time-resolved excitation spectroscopy on single InAs QDs and demonstrate resonance fluorescence with a line-width of $\approx 10\ \mu$eV, by temporally filtering the time-resolved luminescence signal [137].

On a similar GaAs photonic platform with InAs QDs, Schwartz *et al.* demonstrated HBT measurements entirely on chip [161]. The device comprised InAs QDs in GaAs ridge WGs and a directional coupler beamsplitter with integrated NbN SNSPDs, as represented in Fig. 1.13. Light emitted by a resonantly excited QD in a WG was split in a directional coupler beamsplitter and then detected by the on-chip SNSPDs. To effectively suppress the excitation laser stray light, aluminum cover layers were deposited above the SNSPDs and WG regions (buffered

by an oxide layer), allowing operation without the need for spectral filtering or time gating. The single-photon nature of the QD emission was proven under continuous-wave and pulsed excitation, via the on-chip HBT circuit. The detection efficiencies for the two SNSPDs used in the experiment were significantly different, up to ≈ 47 % and ≈ 16 % close to the critical currents, and ≈ 1.8 % and ≈ 21.8 % for the bias level used for the HBT measurement.

While in all the work described above SNSPDs were produced directly onto the final photonic chip, the pick-and-place technique was used in the work of Najafi *et al.* [111] to produce a hybrid SOI integrated photonic circuit chip for photon correlation measurements. The pick-and-place technique here was chosen to circumvent the typically low fabrication yield for SNSPDs, which is limited by nanoscale defects [145, 58]. As suggested in Fig. 1.21(c), the SNSPDs were produced on SiN_x membranes in a separate run than that of the SOI photonic circuit, and then transferred on top of the latter with a tungsten tip. The close proximity between the WG and the SNSPD allowed single-photon detection. This process allowed ten low-jitter detectors to be integrated on one circuit with 100 % device yield. With an average system detection efficiency beyond 10 %, and estimated on-chip detection efficiency of 14 % to 52 % for four detectors operated simultaneously.

Photon-number resolving detectors were also integrated with on-chip waveguides. In the work of Gerrits *et al.*, a tungsten transition-edge sensor (TES) operating in the 1550 nm telecom band, evanescently coupled to a UV-written silica waveguide, was demonstrated [45]. In the experiment, up to five photons were resolved in the guided optical mode (which was closely matched to that of an optical fiber), with a maximum detection efficiency of ≈ 7.2 %. One important consideration regarding the fabricated chip was that the top surface was smooth to less than 1 nm, a critical need to preserve the tungsten superconducting transition temperature. A $T_c \approx 90$ mK was observed, for a 40 nm thick film, and the device was operated at 12 mK in a dilution refrigerator. In later work, Sahin *et al.* demonstrated NbN photon-number-resolving detectors on $GaAs/Al_{0.75}Ga_{0.25}As$ ridge waveguides [144]. Operating at 2.1 K, detection of up to four photons was reported, with a maximum efficiency of 24 % at 1310 nm. The detector featured a series connection of four nanowires, whereas each nanowire represented distinct detecting elements, sensing different parts of the same waveguide mode. The number of triggered nanowires could furthermore be determined from the output voltage. An important factor contributing to lowering of detection efficiencies here was the quality of the sputtered NbN. While sputtering requires high temperature to promote surface diffusion, critical for high film quality, as As-oxide desorption at temperatures above 350 °C led to rougher GaAs surfaces.

As an illustration of the potential for novel applications brought by heterogeneous integration of single-photon detectors, the work of Cheng *et al.* demonstrated a chip-scale integrated photonic single-photon spectrometer, covering a broad wavelength range, spanning from 600 nm to 2000 nm [19]. The spec-

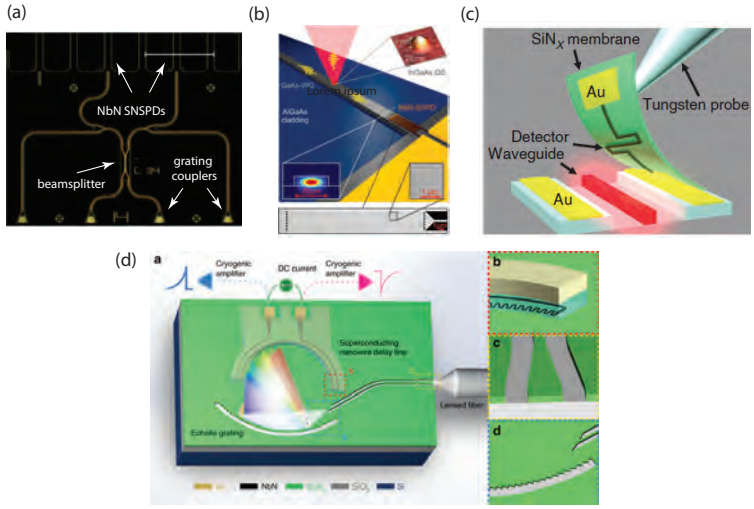

FIGURE 1.21 (a) Integrated silicon photonic beamsplitter with integrated NbN SNSPDs from Schuck *et al.* Ref. [158]. *(Adapted from ref. [158] with permission from Springer Nature)* (b) Representation of the GaAs-based photonic circuit demonstrated from Reithmaier *et al.* [138], which comprised InAs QD single photon sources and NbN SNSPDs. *(Reprinted from ref. [138] with permission from the American Chemical Society.)* (c) Representation of the pick-and-place technique used by Najafi *et al.* [111], to produce a hybrid SOI photonic circuit with NbN SNSPDs. *(Reprinted from ref. [111] with permission from Springer Nature.)* (d) Representation of the integrated photonic spectrometer of Cheng *et al.* ref. [19]. An on-chip focusing echelle grating disperses the incoming, WG-coupled optical signal across the SNSPD. The SNSPD functions as a single-photon detector and a slow microwave delay line, which allows it to map the dispersed photons. *(Reprinted from ref. [19] with permission from Springer Nature.)*

trometer comprised an on-chip, WG-coupled dispersive echelle grating, and a single-element, NbN propagating superconducting nanowire detector, as shown in Fig. 1.21(d). The detector also functioned as a slow-wave microwave transmission line, such that the arrival time-difference for generated signals at its two ends could lead to high resolution spatial mapping of the dispersed photons. The echelle and the WG leading to it was composed of Si_3N_4.

1.6 OUTLOOK

Progress in the field of IQPCs have been considerable but very unequal, depending on the used platform. We propose a comparison between the different explored platforms in order to evaluate the advancement of device integration and provide an outlook on the different challenges inherent to each structure. Table 1.1 gives an overview on the advances of the field, based on the different components and operations to be implemented in an ideal IQPC.

So far, Si-based platforms have seen the fastest and most impressive development of the past decade. The number of optical components integrated into the

Platform	Waveguiding	Beamsplitting	Control of phase	On-chip detection	Boson Sampling	Quantum logic	Deterministic quantum logic	Large scale operations
Si- based chips	Yes	Yes	Yes	Yes	Yes	Yes	No	In progress
GaAs	Yes	Yes	In progress	Yes	No	No	No	No
Diamond-based	Yes	No	No	Yes	No	No	No	No

TABLE 1.1 Accomplished functionalities and the state-of-the art for the platforms reviewed in this section. In progress means that the functionality has been demonstrated as a proof-of-principle but was not confirmed or not reported in an integrated structure.

IQPCs has expanded exponentially over the years, as shown on Fig. 1.22(a) [193]. Development has grown from a single multimode interferometer, used for demonstration of the on-chip Hong-Ou Mandel experiment, to a state-of-the-art large scale IQPC comprising 671 optical components designed for the demonstration of multidimensional entanglement [191]. Recent demonstrations in integrated classical photonics, embedding up to 57 600 photonic switches on chip [163] seem to indicate that further development of very large-scale integrated quantum photonic devices can be expected over the next years. The IQPC will have to rely on the processing of very large number of single photons and will require further efforts in the realization of multiplexed parametric single-photon sources [71, 21]. Such a massive deployment of optical components will also require a significant improvement of the low-loss waveguides at hand [85, 8], for critical applications - such as high-rate boson sampling, efficient generation of cluster states and fault-tolerant quantum computation. Another major technical issue typically encountered, on all platforms, is the rejection of the pump laser addressing the integrated SPSs. Promising solutions involving cascaded microrings [114] and MZIs [125] have recently been proposed and already achieve up to 100 dB rejection.

GaAs IQPCs emerged as the second most reliable platform for on-chip quantum operations. They offer the advantage of relying on potentially deterministic SPS, which are relatively easy to integrate. Almost all of the building blocks have been demonstrated, but the challenge remains in the integration of all the parts, and their good functioning, into the same chip. The recent demonstration of fully integrated basic quantum experiment in a state-of-the-art chip reveals that the technology reached a certain level of maturity [161]. Even if antibunching is demonstrated, it is dramatically degraded by the remaining pump laser. The filtering of the latter is also a well identified issue for the GaAs platform. This might be tackled by on-chip filters, for instance the directional coupler grating filters by Sakata *et al.* [146], implemented on an AlGaAs/GaAs multi-quantum-well platform. An equivalent scheme combining PhC cavities and ridge waveguides has been proposed for the realization of on-chip HOM [28](Fig. 1.22b). This solution allows for an efficient filtering of the excitonic line thanks to the PhC cavity but suffers from typically very lossy interfaces between the photonic crystal structure and the ridge waveguides. Further control of the excitonic emission energy via the DC Stark effect achieved by the introduction p- and n- regions into the PhC. The tunability of the on-chip SPSs is a crucial prerequisite and should be urgently addressed. Even if III-V semiconductor technology might come

second to Si-based IQPC in terms of large-scale integration, very ambitious deterministic quantum logic schemes based on GaAs artificial atoms seem to be reachable today, with the actual state-of-the-art [168](Fig. 1.22c). In order to increase the index contrast, hybrid structures are attracting increasing attention. Since GaAs/SiO2 has a similar index contrast as Si/SiO_2, significant work in this direction has already been accomplished (see Sec. 1.5) and other III-V materials than GaAs are also considered in this context. InP for example might be an attractive candidate, based on its successes in classical photonics. However, the implementation of single-photon sources in this material is so far limited [14], and concerns about decoherence in these structures have to be lifted.

As discussed in Section 1.5, heterogeneous integration offers great potential for circumventing many of the trade-offs that exist in single-material systems. While big strides have been made towards creating IQPCs with quantum emitters, reconfigurable linear optics and single-photon or photon number-resolving detectors, many challenges still remain. Because quantum photonic devices that may operate in the quantum advantage or supremacy regime are expected to require large resources (in terms of numbers of photonic qubits, logical channels, detectors, ancilla photons), methods to produce all such elements in large scale on chip is key. Large-scale reconfigurable waveguide-based linear-optical networks, capable of implementing all possible linear-quantum-optical protocols, have been demonstrated in silicon [15], and can likewise be implemented in a number of other types of materials (such as silicon nitride [180], silicon oxynitride [109, 31], aluminum nitride [187, 197] and lithium niobate [27]) for which mature, top-down fabrication techniques already exist. Scalable incorporation of quantum emitters onto such on-chip networks however constitutes a crucial bottleneck, originating in the wide heterogeneity of quantum emitters properties. Generally, quantum emitters are highly sensitive to various physical factors, such as local fluctuating electric and magnetic fields, phonons, mechanical stress. All such factors taken together lead to significant variations in energy, quantum efficiency, spectral diffusion and coherence of the quantum emitter; their influence must be effectively controlled to ensure sufficient emitter performance for quantum photonic applications. In particular, the effects of fabrication methods upon the quantum emitter's natural characteristics must be carefully considered. In addition, as argued in Sec. 1.3, techniques that allow identification of single quantum emitters with the desirable characteristics within a population before fabrication are a necessity towards scalable fabrication of single-emitter devices. The ability to fully characterize a quantum emitter's location and orientation on a sample, as well as its spectrum, is furthermore critical to ensure efficient emitter coupling to desirable spatial optical modes supported by nanophotonic structures [89]. This in turn has direct influence on the overall device efficiency. While deterministic fabrication of single QD devices in heterogeneous samples has been demonstrated by Schnauber *et al.* [156], a detailed characterization of the selected quantum dots pre-fabrication (regarding dipole momement orientation, quantum efficiency, spectral purity, etc) was not performed. Sig-

nificant advances may take place, with the development of high-throughput single-quantum-emitter spectroscopic characterization techniques.

Another promising approach towards scable integration of quantum emitters was demonstrated by Wan *et al.* [187], in which arrays of nanophotonic diamond waveguides containing deterministically implanted Si and Ge color centers were placed onto AlN photonic circuits through a pick-and place technique. Development of high-throughput pick-and-place techniques could further increase the scalability of such technique.

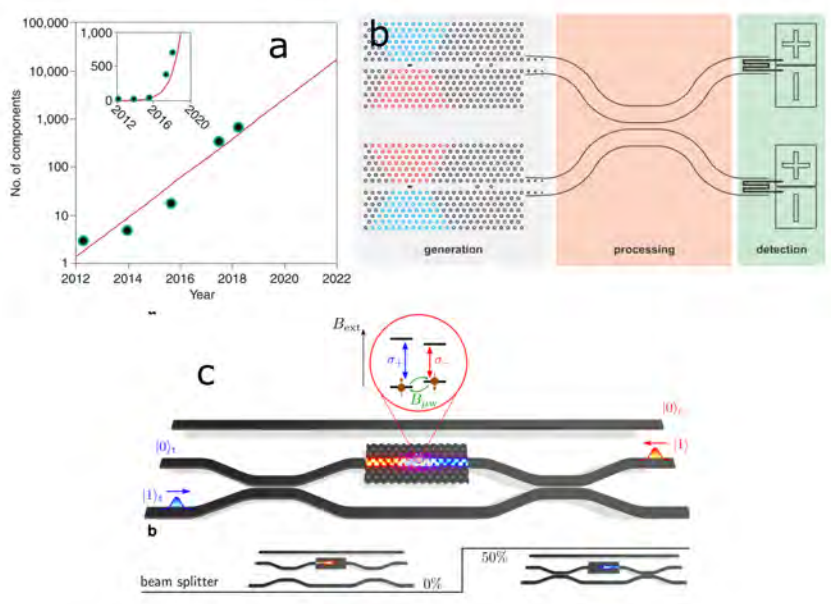

FIGURE 1.22 a) Expansion of the number of components integrated into IQPCs in silicon-based platforms as a function of the years [193]. b) Proposed scheme of a PhC-ridge waveguide structure for the on-chip realization of a HOM experiment [28]. c) Resonator with reverse bias enhancement. d) Proposed scheme of an artificial atom used for implementation of a deterministic CNOT quantum gate and based on a chiral PhC QD-WG system.

1.7 CONCLUSION

In summary, this chapter gives an overview of the basics and current developments in the field of integrated quantum nanophotonics and related fields of modern photonic quantum technology. Important methods, namely the FEM and FDTD approaches for numerical modeling of integrated photonic structures were presented, which are used effectively for the design and understanding of such elements. With regard to the production of integrated photonic circuits, the focus was also on novel methods that enable the deterministic integration of quantum

emitters in waveguide structures. An important method is the in-situ EBL technology platform, which promises a precise and very reproducible integration of quantum emitters in complex circuits and will therefore play an important technological basis for scalable integrated quantum nanophotonics. Furthermore, current approaches and results for photonic circuits based on homogeneous materials such as Si and GaAs were presented. These more traditional approaches were and are still very successful in realizing important sub-functionalities such as linear quantum gates and circuits for boson sampling. They are comparatively easy to fabricate, which makes them particularly attractive for the study of basic physical properties such as the chiral light-matter interaction discussed. Additional functionalities and fully integrated photonic quantum circuits, however, require heterogeneous material integration. In this context, current approaches for heterogeneous quantum circuits were presented, which for example include not only waveguide structures but also single-photon detectors. Furthermore, open questions and challenges were discussed and an outlook on possible future developments was given, which among other things aimed at modular quantum circuits for the implementation of large-scale quantum networks.

BIBLIOGRAPHY

[1] Shahriar Aghaeimeibodi, Boris Desiatov, Je-Hyung Kim, Chang-Min Lee, Mustafa Atabey Buyukkaya, Aziz Karasahin, Christopher J. K. Richardson, Richard P. Leavitt, Marko Lončar, and Edo Waks. Integration of quantum dots with lithium niobate photonics. *Applied Physics Letters*, 113(22):221102, November 2018.

[2] Igor Aharonovich, Stefania Castelletto, Brett C. Johnson, Jeffrey C. McCallum, David A. Simpson, Andrew D. Greentree, and Steven Prawer. Chromium single-photon emitters in diamond fabricated by ion implantation. *Physical Review B*, 81:121201, Mar 2010.

[3] Igor Aharonovich, Dirk Englund, and Milos Toth. Solid-state single-photon emitters. *Nature Photonics*, 10(10):631–641, Sep 2016.

[4] N. Akopian, N. H. Lindner, E. Poem, Y. Berlatzky, J. Avron, D. Gershoni, B. D. Gerardot, and P. M. Petroff. Entangled photon pairs from semiconductor quantum dots. *Physical Review Letters*, 96:130501, Apr 2006.

[5] M. Arcari, I. Söllner, A. Javadi, S. Lindskov Hansen, S. Mahmoodian, J. Liu, H. Thyrrestrup, E. H. Lee, J. D. Song, S. Stobbe, and P. Lodahl. Near-unity coupling efficiency of a quantum emitter to a photonic crystal waveguide. *Physical Review Letters*, 113:093603, Aug 2014.

[6] Frank Arute, Kunal Arya, Ryan Babbush, Dave Bacon, Joseph C. Bardin, Rami Barends, Rupak Biswas, Sergio Boixo, Fernando G. S. L. Brandao, David A. Buell, Brian Burkett, Yu Chen, Zijun Chen, Ben Chiaro, Roberto Collins, William Courtney, Andrew Dunsworth, Edward Farhi, Brooks Foxen, Austin Fowler, Craig Gidney, Marissa Giustina, Rob Graff, Keith Guerin, Steve Habegger, Matthew P. Harrigan, Michael J. Hartmann, Alan Ho, Markus Hoffmann, Trent Huang, Travis S. Humble, Sergei V. Isakov, Evan Jeffrey, Zhang Jiang, Dvir Kafri, Kostyantyn Kechedzhi, Julian Kelly, Paul V. Klimov, Sergey Knysh, Alexander Korotkov, Fedor Kostritsa, David Landhuis, Mike Lindmark, Erik Lucero, Dmitry Lyakh, Salvatore Mandrà, Jarrod R. McClean, Matthew McEwen, Anthony Megrant, Xiao Mi, Kristel Michielsen, Masoud Mohseni, Josh Mutus, Ofer Naaman, Matthew Neeley, Charles Neill, Murphy Yuezhen Niu, Eric Ostby, Andre Petukhov, John C. Platt, Chris Quintana, Eleanor G. Rieffel, Pedram Roushan, Nicholas C. Rubin, Daniel Sank, Kevin J. Satzinger, Vadim Smelyanskiy, Kevin J. Sung, Matthew D. Trevithick, Amit Vainsencher, Benjamin Villalonga, Theodore White, Z. Jamie Yao, Ping Yeh, Adam Zalcman, Hartmut Neven, and John M. Martinis. Quantum supremacy using a programmable superconducting processor. *Nature*, 574(7779):505–510, Oct 2019.

[7] Thang Ba Hoang, Johannes Beetz, Leonardo Midolo, Matthias Skacel, Matthias Lermer, Martin Kamp, Sven Höfling, Laurent Balet, Nicolas Chauvin, and Andrea Fiore. Enhanced spontaneous emission from quantum dots in short photonic crystal waveguides. *Applied Physics Letters*, 100(6):061122, 2012.

[8] Jared F. Bauters, Martijn J. R. Heck, Demis D. John, Jonathon S. Barton, Christiaan M. Bruinink, Arne Leinse, René G. Heideman, Daniel J. Blumenthal, and John E. Bowers. Planar waveguides with less than 0.1 db/m propagation loss fabricated with wafer bonding. *Optics Express*, 19(24):24090–24101, Nov 2011.

[9] Jean-Pierre Berenger. A perfectly matched layer for the absorption of electromagnetic waves. *Journal of Computational Physics*, 114(2):185 – 200, 1994.

[10] Aleksander Bogucki, Łukasz Zinkiewicz, Wojciech Pacuski, Piotr Wasylczyk, and Piotr Kossacki. Optical fiber micro-connector with nanometer positioning precision for rapid prototyping of photonic devices. *Optics Express*, 26(9):11513–11518, Apr 2018.

[11] Lucas Bremer, Ksenia Weber, Sarah Fischbach, Simon Thiele, Marco Schmidt, Arsenty Kakganskiy, Sven Rodt, Alois Herkommer, Marc Sartison, Simone Luca Portalupi, Peter

Michler, Harald Giessen, and Stephan Reitzenstein. Quantum dot single-photon emission coupled into single-mode fibers with 3d printed micro-objectives. *arxiv:2005.11198*, 2020.

[12] Hans J. Briegel and Robert Raussendorf. Persistent entanglement in arrays of interacting particles. *Physical Review Letters*, 86:910–913, Jan 2001.

[13] Matthew A. Broome, Alessandro Fedrizzi, Saleh Rahimi-Keshari, Justin Dove, Scott Aaronson, Timothy C. Ralph, and Andrew G. White. Photonic boson sampling in a tunable circuit. *Science*, 339(6121):794–798, 2013.

[14] Sonia Buckley, Kelley Rivoire, and Jelena Vučković. Engineered quantum dot single-photon sources. *Reports on Progress in Physics*, 75(12):126503, nov 2012.

[15] Jacques Carolan, Christopher Harrold, Chris Sparrow, Enrique Martín-López, Nicholas J. Russell, Joshua W. Silverstone, Peter J. Shadbolt, Nobuyuki Matsuda, Manabu Oguma, Mikitaka Itoh, Graham D. Marshall, Mark G. Thompson, Jonathan C. F. Matthews, Toshikazu Hashimoto, Jeremy L. O'Brien, and Anthony Laing. Universal linear optics. *Science*, 349(6249):711–716, 2015.

[16] Jacques Carolan, Christopher Harrold, Chris Sparrow, Enrique Martín-López, Nicholas J. Russell, Joshua W. Silverstone, Peter J. Shadbolt, Nobuyuki Matsuda, Manabu Oguma, Mikitaka Itoh, Graham D. Marshall, Mark G. Thompson, Jonathan C. F. Matthews, Toshikazu Hashimoto, Jeremy L. O'Brien, and Anthony Laing. Universal linear optics. *Science*, 349(6249):711–716, 2015.

[17] Jacques Carolan, Jasmin D. A. Meinecke, Peter J. Shadbolt, Nicholas J. Russell, Nur Ismail, Kerstin Wörhoff, Terry Rudolph, Mark G. Thompson, Jeremy L. O'Brien, Jonathan C. F. Matthews, and Anthony Laing. On the experimental verification of quantum complexity in linear optics. *Nature Photonics*, 8(8):621–626, Aug 2014.

[18] Lin Chang, Andreas Boes, Xiaowen Guo, Daryl T. Spencer, M. J. Kennedy, Jon D. Peters, Nicolas Volet, Jeff Chiles, Abijith Kowligy, Nima Nader, Daniel D. Hickstein, Eric J. Stanton, Scott A. Diddams, Scott B. Papp, and John E. Bowers. Heterogeneously integrated gaas waveguides on insulator for efficient frequency conversion. *Laser and Photonics Reviews*, 12(10):1800149, 2018.

[19] Risheng Cheng, Chang-Ling Zou, Xiang Guo, Sihao Wang, Xu Han, and Hong X. Tang. Broadband on-chip single-photon spectrometer. *Nature Communications*, 10(1):4104, September 2019.

[20] R. J. Coles, D. M. Price, J. E. Dixon, B. Royall, E. Clarke, P. Kok, M. S. Skolnick, A. M. Fox, and M. N. Makhonin. Chirality of nanophotonic waveguide with embedded quantum emitter for unidirectional spin transfer. *Nature Communications*, 7(1):11183, Mar 2016.

[21] M. Collins, C. Xiong, and I. et al. Rey. Integrated spatial multiplexing of heralded single-photon sources. *Nature Communication*, 4(7198):2582, 2013.

[22] A. Crespi, R. Ramponi, and R. et al. Osellame. Integrated photonic quantum gates for polarization qubits. *Nature Communication*, 2(7948):566, 2015.

[23] Marcelo Davanco, Jin Liu, Luca Sapienza, Chen-Zhao Zhang, José Vinícius De Miranda Cardoso, Varun Verma, Richard Mirin, Sae Woo Nam, Liu Liu, and Kartik Srinivasan. Heterogeneous integration for on-chip quantum photonic circuits with single quantum dot devices. *Nature Communications*, 8(1):889, Oct 2017.

[24] Raphael S. Daveau, Krishna C. Balram, Tommaso Pregnolato, Jin Liu, Eun H. Lee, Jin D. Song, Varun Verma, Richard Mirin, Sae Woo Nam, Leonardo Midolo, Søren Stobbe, Kartik Srinivasan, and Peter Lodahl. Efficient fiber-coupled single-photon source based on quantum dots in a photonic-crystal waveguide. *Optica*, 4(2):178–184, Feb 2017.

[25] Jakob Rosenkrantz de Lasson, Lars Hagedorn Frandsen, Philipp Gutsche, Sven Burger, Oleksiy S. Kim, Olav Breinbjerg, Aliaksandra Ivinskaya, Fengwen Wang, Ole Sigmund,

Teppo Häyrynen, Andrei V. Lavrinenko, Jesper Mørk, and Niels Gregersen. Benchmarking five numerical simulation techniques for computing resonance wavelengths and quality factors in photonic crystal membrane line defect cavities. *Optics Express*, 26(9):11366–11392, Apr 2018.

[26] Parag B. Deotare, Murray W. McCutcheon, Ian W. Frank, Mughees Khan, and Marko Lončar. High quality factor photonic crystal nanobeam cavities. *Applied Physics Letters*, 94(12):121106, 2009.

[27] Boris Desiatov, Amirhassan Shams-Ansari, Mian Zhang, Cheng Wang, and Marko Lončar. Ultra-low-loss integrated visible photonics using thin-film lithium niobate. *Optica*, 6(3):380–384, March 2019.

[28] Christof P. Dietrich, Andrea Fiore, Mark G. Thompson, Martin Kamp, and Sven Höfling. Gaas integrated quantum photonics: Towards compact and multi-functional quantum photonic integrated circuits. *Laser Photonics Rev.*, 10(6):870–894, 2016.

[29] Xing Ding, Yu He, Z.-C. Duan, Niels Gregersen, M.-C. Chen, S. Unsleber, S. Maier, Christian Schneider, Martin Kamp, Sven Höfling, Chao-Yang Lu, and Jian-Wei Pan. On-demand single photons with high extraction efficiency and near-unity indistinguishability from a resonantly driven quantum dot in a micropillar. *Physical Review Letters*, 116(2):020401, jan 2016.

[30] A. Dousse, L. Lanco, J. Suffczyński, E. Semenova, A. Miard, A. Lemaître, I. Sagnes, C. Roblin, J. Bloch, and P. Senellart. Controlled light-matter coupling for a single quantum dot embedded in a pillar microcavity using far-field optical lithography. *Physical Review Letters*, 101:267404, Dec 2008.

[31] D. J. P. Ellis, A. J. Bennett, C. Dangel, J. P. Lee, J. P. Griffiths, T. A. Mitchell, T.-K. Paraiso, P. Spencer, D. A. Ritchie, and A. J. Shields. Independent indistinguishable quantum light sources on a reconfigurable photonic integrated circuit. *Applied Physics Letters*, 112(21):211104, May 2018.

[32] Ali W. Elshaari, Efe Büyüközer, Iman Esmaeil Zadeh, Thomas Lettner, Peng Zhao, Eva Schöll, Samuel Gyger, Michael E. Reimer, Dan Dalacu, Philip J. Poole, Klaus D. Jöns, and Val Zwiller. Strain-Tunable Quantum Integrated Photonics. *Nano Letters*, 18(12):7969–7976, December 2018.

[33] Ali W. Elshaari, Iman Esmaeil Zadeh, Andreas Fognini, Michael E. Reimer, Dan Dalacu, Philip J. Poole, Val Zwiller, and Klaus D. Jöns. On-chip single photon filtering and multiplexing in hybrid quantum photonic circuits. *Nature Communications*, 8(1):379–, 2017.

[34] Ali W. Elshaari, Iman Esmaeil Zadeh, Andreas Fognini, Michael E. Reimer, Dan Dalacu, Philip J. Poole, Val Zwiller, and Klaus D. J´ons. On-chip single photon filtering and multiplexing in hybrid quantum photonic circuits. *Nature Communications*, 8(1):379, 2017.

[35] Erman Engin, Damien Bonneau, Chandra M. Natarajan, Alex S. Clark, M. G. Tanner, R. H. Hadfield, Sanders N. Dorenbos, Val Zwiller, Kazuya Ohira, Nobuo Suzuki, Haruhiko Yoshida, Norio Iizuka, Mizunori Ezaki, Jeremy L. O'Brien, and Mark G. Thompson. Photon pair generation in a silicon micro-ring resonator with reverse bias enhancement. *Optics Express*, 21(23):27826–27834, Nov 2013.

[36] A. Javadi et al. Spin-photon interface and spin-controlled photon switching in a nanobeam waveguide. *Nature Nanotechnology*, 13:398–403, 2018.

[37] Alexander W. Fang, Hyundai Park, Oded Cohen, Richard Jones, Mario J. Paniccia, and John E. Bowers. Electrically pumped hybrid AlGaInAs-silicon evanescent laser. *Optics Express*, 14(20):9203–9210, October 2006.

[38] Andrei Faraon, Ilya Fushman, Dirk Englund, Nick Stoltz, Pierre Petroff, and Jelena Vučković. Dipole induced transparency in waveguide coupled photonic crystal cavities. *Optics Express*, 16(16):12154–12162, Aug 2008.

[39] Andrei Faraon, Charles Santori, Zhihong Huang, Kai-Mei C Fu, Victor M Acosta, David Fattal, and Raymond G Beausoleil. Quantum photonic devices in single-crystal diamond. *New Journal of Physics*, 15(2):025010, feb 2013.

[40] S. Fattah, T. B. Hoang, L. Midolo, C. P. Dietrich, L. H. Li, E. H. Linfield, J. F. P. Schouwenberg, T. Xia, F. M. Pagliano, F. W. M. van Otten, and A. Fiore. Efficient coupling of single photons to ridge-waveguide photonic integrated circuits. *Applied Physics Letters*, 102(13):131105, 2013.

[41] Sarah Fischbach, Alexander Schlehahn, Alexander Thoma, Nicole Srocka, Timo Gissibl, Simon Ristok, Simon Thiele, Arsenty Kaganskiy, André Strittmatter, Tobias Heindel, et al. Single quantum dot with microlens and 3d-printed micro-objective as integrated bright single-photon source. *ACS Photonics*, 4(6):1327–1332, 2017.

[42] Fulvio Flamini, Lorenzo Magrini, Adil S. Rab, Nicolò Spagnolo, Vincenzo D'Ambrosio, Paolo Mataloni, Fabio Sciarrino, Tommaso Zandrini, Andrea Crespi, Roberta Ramponi, and Roberto Osellame. Thermally reconfigurable quantum photonic circuits at telecom wavelength by femtosecond laser micromachining. *Light: Science & Applications*, 4(11):e354–e354, Nov 2015.

[43] T Gaebel, I Popa, A Gruber, M Domhan, F Jelezko, and J Wrachtrup. Stable single-photon source in the near infrared. *New Journal of Physics*, 6:98–98, jul 2004.

[44] I. M. Georgescu, S. Ashhab, and Franco Nori. Quantum simulation. *Review of Modern Physics*, 86:153–185, Mar 2014.

[45] Thomas Gerrits, Nicholas Thomas-Peter, James C. Gates, Adriana E. Lita, Benjamin J. Metcalf, Brice Calkins, Nathan A. Tomlin, Anna E. Fox, Antía Lamas Linares, Justin B. Spring, Nathan K. Langford, Richard P. Mirin, Peter G. R. Smith, Ian A. Walmsley, and Sae Woo Nam. On-chip, photon-number-resolving, telecommunication-band detectors for scalable photonic information processing. *Physical Review A*, 84:060301, Dec 2011.

[46] Davide Grassani, Stefano Azzini, Marco Liscidini, Matteo Galli, Michael J. Strain, Marc Sorel, J. E. Sipe, and Daniele Bajoni. Micrometer-scale integrated silicon source of time-energy entangled photons. *Optica*, 2(2):88–94, Feb 2015.

[47] M. Gschrey, F. Gericke, A. Schüssler, R. Schmidt, J.-H. Schulze, T. Heindel, S. Rodt, A. Strittmatter, and S. Reitzenstein. In situ electron-beam lithography of deterministic single-quantum-dot mesa-structures using low-temperature cathodoluminescence spectroscopy. *Applied Physics Letters*, 102(25):251113, 2013.

[48] M. Gschrey, A. Thoma, P. Schnauber, M. Seifried, R. Schmidt, B. Wohlfeil, L. Krüger, J. H. Schulze, T. Heindel, S. Burger, F. Schmidt, A. Strittmatter, S. Rodt, and S Reitzenstein. Highly indistinguishable photons from deterministic quantum-dot microlenses utilizing three-dimensional in situ electron-beam lithography. *Nature Communications*, 6:7662, Jul 2015.

[49] Manuel Gschrey, Ronny Schmidt, Arsenty Kaganskiy, Sven Rodt, and Stephan Reitzenstein. Study of high-resolution electron-beam resists for applications in low-temperature lithography. *Journal of Vacuum Science & Technology B, Nanotechnology and Microelectronics: Materials, Processing, Measurement, and Phenomena*, 32(6):061601, 2014.

[50] Manuel Gschrey, Ronny Schmidt, Jan-Hindrik Schulze, André Strittmatter, Sven Rodt, and Stephan Reitzenstein. Resolution and alignment accuracy of low-temperature in situ electron beam lithography for nanophotonic device fabrication. *Journal of Vacuum Science & Technology B, Nanotechnology and Microelectronics: Materials, Processing, Measurement, and Phenomena*, 33(2):021603, 2015.

[51] Manuel Gschrey, Ronny Schmidt, Jan-Hindrik Schulze, Andre Strittmatter, Sven Rodt, and Stephan Reitzenstein. Resolution and alignment accuracy of low-temperature in situ electron beam lithography for nanophotonic device fabrication. *Journal of Vacuum Science &*

Technology B, 33(2):021603, 2015.

[52] Craig S. Hamilton, Regina Kruse, Linda Sansoni, Sonja Barkhofen, Christine Silberhorn, and Igor Jex. Gaussian boson sampling. *Physical Review Letters*, 119:170501, Oct 2017.

[53] Nicholas C. Harris, Darius Bunandar, Mihir Pant, Greg R. Steinbrecher, Jacob Mower, Mihika Prabhu, Tom Baehr-Jones, Michael Hochberg, and Dirk Englund. Large-scale quantum photonic circuits in silicon. *Nanophotonics*, 5(3):456 – 468, 2016.

[54] Nicholas C. Harris, Davide Grassani, Angelica Simbula, Mihir Pant, Matteo Galli, Tom Baehr-Jones, Michael Hochberg, Dirk Englund, Daniele Bajoni, and Christophe Galland. Integrated source of spectrally filtered correlated photons for large-scale quantum photonic systems. *Physical Review X*, 4:041047, Dec 2014.

[55] Nicholas C. Harris, Gregory R. Steinbrecher, Mihika Prabhu, Yoav Lahini, Jacob Mower, Darius Bunandar, Changchen Chen, Franco N. C. Wong, Tom Baehr-Jones, Michael Hochberg, Seth Lloyd, and Dirk Englund. Quantum transport simulations in a programmable nanophotonic processor. *Nature Photonics*, 11(7):447–452, Jul 2017.

[56] B. J. M. Hausmann, I. B. Bulu, P. B. Deotare, M. McCutcheon, V. Venkataraman, M. L. Markham, D. J. Twitchen, and M. Loncar. Integrated high-quality factor optical resonators in diamond. *Nano Letters*, 13(5):1898–1902, 2013.

[57] Birgit J. M. Hausmann, Brendan Shields, Qimin Quan, Patrick Maletinsky, Murray McCutcheon, Jennifer T. Choy, Tom M. Babinec, Alexander Kubanek, Amir Yacoby, Mikhail D. Lukin, and Marko Loncar. Integrated diamond networks for quantum nanophotonics. *Nano Letters*, 12(3):1578–1582, 2012.

[58] L. Heeres, R.and Kouwenhoven and V. Zwiller. On-chip generation of high-dimensional entangled quantum states and their coherent control. *Nature Nanotechnology*, 8(7948):719–722, 2013.

[59] T. Heindel, A. Thoma, M. von Helversen, M. Schmidt, A. Schlehahn, M. Gschrey, P. Schnauber, J. H. Schulze, A. Strittmatter, J. Beyer, S. Rodt, A. Carmele, A. Knorr, and S. Reitzenstein. A bright triggered twin-photon source in the solid state. *Nature Communications*, 8:14870, April 2017.

[60] B. Hensen, H. Bernien, A. E. Dréau, A. Reiserer, N. Kalb, M. S. Blok, J. Ruitenberg, R. F. L. Vermeulen, R. N. Schouten, C. Abellán, W. Amaya, V. Pruneri, M. W. Mitchell, M. Markham, D. J. Twitchen, D. Elkouss, S. Wehner, T. H. Taminiau, and R. Hanson. Loophole-free bell inequality violation using electron spins separated by 1.3 kilometres. *Nature*, 526(7575):682–686, Oct 2015.

[61] Stefan Hepp, Stephanie Bauer, Florian Hornung, Mario Schwartz, Simone L. Portalupi, Michael Jetter, and Peter Michler. Bragg grating cavities embedded into nano-photonic waveguides for purcell enhanced quantum dot emission. *Optics Express*, 26(23):30614–30622, Nov 2018.

[62] Mark P. Hiscocks, Kumaravelu Ganesan, Brant C. Gibson, Shane T. Huntington, François Ladouceur, and Steven Prawer. Diamond waveguides fabricated by reactive ion etching. *Optics Express*, 16(24):19512–19519, Nov 2008.

[63] Michael Hochberg and Tom Baehr-Jones. Towards fabless silicon photonics. *Nature Photonics*, 4(8):492, 2010.

[64] Rolf Horn, Payam Abolghasem, Bhavin J. Bijlani, Dongpeng Kang, A. S. Helmy, and Gregor Weihs. Monolithic source of photon pairs. *Physical Review Letters*, 108:153605, Apr 2012.

[65] Takayuki Iwasaki, Fumitaka Ishibashi, Yoshiyuki Miyamoto, Yuki Doi, Satoshi Kobayashi, Takehide Miyazaki, Kosuke Tahara, Kay D. Jahnke, Lachlan J. Rogers, Boris Naydenov, Fedor Jelezko, Satoshi Yamasaki, Shinji Nagamachi, Toshiro Inubushi, Norikazu Mizuochi, and Mutsuko Hatano. Germanium-vacancy single color centers in diamond. *Scientific*

Reports, 5(1):12882, Aug 2015.

[66] A. Javadi, I. Söllner, M. Arcari, S. Lindskov Hansen, L. Midolo, S. Mahmoodian, G Kirsanske, T. Pregnolato, E. H. Lee, J. D. Song, S. Stobbe, and P. Lodahl. Single-photon non-linear optics with a quantum dot in a waveguide. *Nature Communications*, 6:8655, October 2015.

[67] Klaus D Jöns, Ulrich Rengstl, Markus Oster, Fabian Hargart, Matthias Heldmaier, Samir Bounouar, Sven M Ulrich, Michael Jetter, and Peter Michler. Monolithic on-chip integration of semiconductor waveguides, beamsplitters and single-photon sources. *Journal of Physics D: Applied Physics*, 48(8):085101, feb 2015.

[68] Arsenty Kaganskiy, Manuel Gschrey, Alexander Schlehahn, Ronny Schmidt, Jan-Hindrik Schulze, Tobias Heindel, André Strittmatter, Sven Rodt, and Stephan Reitzenstein. Advanced in-situ electron-beam lithography for deterministic nanophotonic device processing. *Review of Scientific Instruments*, 86(7):073903, 2015.

[69] Arsenty Kaganskiy, Tobias Heuser, Ronny Schmidt, Sven Rodt, and Stephan Reitzenstein. Csar 62 as negative-tone resist for high-contrast e-beam lithography at temperatures between 4 k and room temperature. *Journal of Vacuum Science & Technology B, Nanotechnology and Microelectronics: Materials, Processing, Measurement, and Phenomena*, 34(6):061603, 2016.

[70] Oliver Kahl, Simone Ferrari, Patrik Rath, Andreas Vetter, Christoph Nebel, and Wolfram H. P. Pernice. High efficiency on-chip single-photon detection for diamond nanophotonic circuits. *J. Lightwave Technol.*, 34(2):249–255, Jan 2016.

[71] F. Kaneda and P. G. Kwiat. High-efficiency single-photon generation via large-scale active time multiplexing. *Science Advances*, 5(10), 2019.

[72] Ryota Katsumi, Yasutomo Ota, Masahiro Kakuda, Satoshi Iwamoto, and Yasuhiko Arakawa. Transfer-printed single-photon sources coupled to wire waveguides. *Optica*, 5(6):691–694, June 2018.

[73] Ryota Katsumi, Yasutomo Ota, Alto Osada, Takeyoshi Tajiri, Takuto Yamaguchi, Masahiro Kakuda, Satoshi Iwamoto, Hidefumi Akiyama, and Yasuhiko Arakawa. In situ wavelength tuning of quantum-dot single-photon sources integrated on a cmos-processed silicon waveguide. *Applied Physics Letters*, 116(4):041103, 2020.

[74] Ryota Katsumi, Yasutomo Ota, Alto Osada, Takuto Yamaguchi, Takeyoshi Tajiri, Masahiro Kakuda, Satoshi Iwamoto, Hidefumi Akiyama, and Yasuhiko Arakawa. Quantum-dot single-photon source on a CMOS silicon photonic chip integrated using transfer printing. *APL Photonics*, 4(3):036105, March 2019.

[75] Svetlana Khasminskaya, Felix Pyatkov, Karolina Słowik, Simone Ferrari, Oliver Kahl, Vadim Kovalyuk, Patrik Rath, Andreas Vetter, Frank Hennrich, Manfred M. Kappes, and et al. Fully integrated quantum photonic circuit with an electrically driven light source. *Nature Photonics*, 10(11):727–732, Sep 2016.

[76] Je-Hyung Kim, Shahriar Aghaeimeibodi, Christopher J. K. Richardson, Richard P. Leavitt, Dirk Englund, and Edo Waks. Hybrid integration of solid-state quantum emitters on a silicon photonic chip. *Nano Letters*, 17(12):7394–7400, 2017.

[77] Gabija Kiršanskė, Henri Thyrrestrup, Raphaël S. Daveau, Chris L. Dreeßen, Tommaso Pregnolato, Leonardo Midolo, Petru Tighineanu, Alisa Javadi, Søren Stobbe, Rüdiger Schott, Arne Ludwig, Andreas D. Wieck, Suk In Park, Jin D. Song, Andreas V. Kuhlmann, Immo Söllner, Matthias C. Löbl, Richard J. Warburton, and Peter Lodahl. Indistinguishable and efficient single photons from a quantum dot in a planar nanobeam waveguide. *Physical Review B*, 96:165306, Oct 2017.

[78] E. Knill, R. Laflamme, and G. J. Milburn. A scheme for efficient quantum computation with linear optics. *Nature*, 409(6816):46–52, Jan 2001.

[79] Tin Komljenovic, Duanni Huang, Paolo Pintus, Minh A. Tran, Michael L. Davenport, and John E. Bowers. Photonic Integrated Circuits Using Heterogeneous Integration on Silicon. *Proceedings of the IEEE*, 106(12):2246–2257, December 2018.

[80] M. Kues, C. Reimer, and P. et al. Roztocki. On-chip generation of high-dimensional entangled quantum states and their coherent control. *Nature*, 546(7948):622–626, 2017.

[81] Andreas V. Kuhlmann, Jonathan H. Prechtel, Julien Houel, Arne Ludwig, Dirk Reuter, Andreas D. Wieck, and Richard J. Warburton. Transform-limited single photons from a single quantum dot. *Nature Communications*, 6(1):8204, Sep 2015.

[82] A. Laucht, S. Pütz, T. Günthner, N. Hauke, R. Saive, S. Frédérick, M. Bichler, M.-C. Amann, A. W. Holleitner, M. Kaniber, and J. J. Finley. A waveguide-coupled on-chip single-photon source. *Physical Review X*, 2:011014, Mar 2012.

[83] G. Lecamp, P. Lalanne, and J. P. Hugonin. Very large spontaneous-emission β factors in photonic-crystal waveguides. *Physical Review Letters*, 99:023902, Jul 2007.

[84] J. L. Leclercq, P. Rojo-Romeo, C. Seassal, J. Mouette, X. Letartre, and P. Viktorovitch. 3d structuring of multilayer suspended membranes including 2d photonic crystal structures. *Journal of Vacuum Science & Technology B: Microelectronics and Nanometer Structures Processing, Measurement, and Phenomena*, 21(6):2903–2906, 2003.

[85] Guoliang Li, Jin Yao, Hiren Thacker, Attila Mekis, Xuezhe Zheng, Ivan Shubin, Ying Luo, Jin hyoung Lee, Kannan Raj, John E. Cunningham, and Ashok V. Krishnamoorthy. Ultralow-loss, high-density soi optical waveguide routing for macrochip interconnects. *Optics Express*, 20(11):12035–12039, May 2012.

[86] Qing Li, Marcelo Davanco, and Kartik Srinivasan. Efficient and low-noise single-photon-level frequency conversion interfaces using silicon nanophotonics. *Nature Photonics*, 10(6):406–414, June 2016.

[87] Feng Liu, Alistair J. Brash, John O'Hara, Luis M. P. P. Martins, Catherine L. Phillips, Rikki J. Coles, Benjamin Royall, Edmund Clarke, Christopher Bentham, Nikola Prtljaga, Igor E. Itskevich, Luke R. Wilson, Maurice S. Skolnick, and A. Mark Fox. High purcell factor generation of indistinguishable on-chip single photons. *Nature Nanotechnology*, 13(9):835–840, Sep 2018.

[88] Jin Liu, Rongbin Su, Yuming Wei, Beimeng Yao, Saimon Filipe Covre da Silva, Ying Yu, Jake Iles-Smith, Kartik Srinivasan, Armando Rastelli, Juntao Li, and Xuehua Wang. A solid-state source of strongly entangled photon pairs with high brightness and indistinguishability. *Nature Nanotechnology*, 14(6):586–593, Jun 2019.

[89] Peter Lodahl, Sahand Mahmoodian, and Søren Stobbe. Interfacing single photons and single quantum dots with photonic nanostructures. *Review of Modern Physics*, 87:347–400, May 2015.

[90] Peter Lodahl, Sahand Mahmoodian, Søren Stobbe, Arno Rauschenbeutel, Philipp Schneeweiss, Jürgen Volz, Hannes Pichler, and Peter Zoller. Chiral quantum optics. *Nature*, 541(7638):473–480, Jan 2017.

[91] J. C. Loredo, M. A. Broome, P. Hilaire, O. Gazzano, I. Sagnes, A. Lemaitre, M. P. Almeida, P. Senellart, and A. G. White. Boson sampling with single-photon fock states from a bright solid-state source. *Physical Review Letters*, 118:130503, Mar 2017.

[92] X Lu, Li, Westly Q, and D A et al. Chip-integrated visible-telecom entangled photon pair source for quantum communication. *Nature Physics*, 15(7198):373–381, 2019.

[93] A. P. Lund, A. Laing, S. Rahimi-Keshari, T. Rudolph, J. L. O'Brien, and T. C. Ralph. Boson sampling from a gaussian state. *Physical Review Letters*, 113:100502, Sep 2014.

[94] T. Lund-Hansen, S. Stobbe, B. Julsgaard, H. Thyrrestrup, T. Sünner, M. Kamp, A. Forchel, and P. Lodahl. Experimental realization of highly efficient broadband coupling of single

quantum dots to a photonic crystal waveguide. *Physical Review Letters*, 101:113903, Sep 2008.

[95] I. J. Luxmoore, N. A. Wasley, A. J. Ramsay, A. C. T. Thijssen, R. Oulton, M. Hugues, A. M. Fox, and M. S. Skolnick. Optical control of the emission direction of a quantum dot. *Applied Physics Letters*, 103(24):241102, 2013.

[96] I. J. Luxmoore, N. A. Wasley, A. J. Ramsay, A. C. T. Thijssen, R. Oulton, M. Hugues, S. Kasture, V. G. Achanta, A. M. Fox, and M. S. Skolnick. Interfacing spins in an InGaAs quantum dot to a semiconductor waveguide circuit using emitted photons. *Physical Review Letters*, 110(3), Jan 2013.

[97] Maxim N. Makhonin, James E. Dixon, Rikki J. Coles, Ben Royall, Isaac J. Luxmoore, Edmund Clarke, Maxime Hugues, Maurice S. Skolnick, and A. Mark Fox. Waveguide coupled resonance fluorescence from on-chip quantum emitter. *Nano Letters*, 14(12):6997–7002, 2014.

[98] V. S. C. Manga Rao and S. Hughes. Single quantum-dot purcell factor and β factor in a photonic crystal waveguide. *Physical Review B*, 75:205437, May 2007.

[99] Igor L. Markov, Aneeqa Fatima, Sergei V. Isakov, and Sergio Boixo. Quantum supremacy is both closer and farther than it appears, arxiv:1807.10749, 2018.

[100] Graham D. Marshall, Alberto Politi, Jonathan C. F. Matthews, Peter Dekker, Martin Ams, Michael J. Withford, and Jeremy L. O'Brien. Laser written waveguide photonic quantum circuits. *Optics Express*, 17(15):12546–12554, Jul 2009.

[101] G Masada, K Miyata, A Politi, T Hashimoto, J L O'Brien, and A Furusawa. Continuous-variable entanglement on a chip. *Nature Photonics*, 9(7198):319, 2015.

[102] Gary S. May and Simon M. Sze. *Fundamentals of Semiconductor Fabrication*, volume 1. Wiley, Weinheim, 2003.

[103] B. Metcalf, J. Spring, P. Humphreys, Nicholas Thomas-Peter, Marco Barbieri, W. Steven Kolthammer, Xian-Min Jin, Nathan K . Langford, Dmytro Kundys, James C. Gates, Brian J. Smith, Peter G. R. Smith, and Ian A. Walmsley. Quantum teleportation on a photonic chip. *Nature Photonics*, 8:770–774, 2014.

[104] P. Michler, A. Kiraz, C. Becher, W. V. Schoenfeld, P. M. Petroff, Lidong Zhang, E. Hu, and A. Imamoglu. A quantum dot single-photon turnstile device. *Science*, 290(5500):2282–2285, 2000.

[105] L Midolo, T Pregnolato, G Kirsanske, and S Stobbe. Soft-mask fabrication of gallium arsenide nanomembranes for integrated quantum photonics. *Nanotechnology*, 26(48):484002, nov 2015.

[106] Sara L. Mouradian, Tim Schröder, Carl B. Poitras, Luozhou Li, Jordan Goldstein, Edward H. Chen, Michael Walsh, Jaime Cardenas, Matthew L. Markham, Daniel J. Twitchen, Michal Lipson, and Dirk Englund. Scalable Integration of Long-Lived Quantum Memories into a Photonic Circuit. *Physical Review X*, 5(3):031009, July 2015.

[107] Paweł Mrowinski, Peter Schnauber, Philipp Gutsche, Arsenty Kaganskiy, Johannes Schall, Sven Burger, Sven Rodt, and Stephan Reitzenstein. Directional emission of a deterministically fabricated quantum dot–bragg reflection multimode waveguide system. *ACS Photonics*, 6(9):2231–2237, 2019.

[108] A. Muller, E. B. Flagg, P. Bianucci, X. Y. Wang, D. G. Deppe, W. Ma, J. Zhang, G. J. Salamo, M. Xiao, and C. K. Shih. Resonance fluorescence from a coherently driven semiconductor quantum dot in a cavity. *Physical Review Letters*, 99:187402, Nov 2007.

[109] E. Murray, D. J. P. Ellis, T. Meany, F. F. Floether, J. P. Lee, J. P. Griffiths, G. A. C. Jones, I. Farrer, D. A. Ritchie, A. J. Bennett, and A. J. Shields. Quantum photonics hybrid integration platform. *Applied Physics Letters*, 107(17), 2015.

[110] Anna Musial, Kinga Zolnacz, Nicole Srocka, Oleh Kravets, Jan Große, Jacek Olszewski, Krzysztof Poturaj, Grzegorz Wojcik, Pawel Mergo, Kamil Dybka, et al. Plug&play fibre-coupled 73 khz single-photon source operating in the telecom o-band. *Advanced Quantum Technologies*, page 202000018, 2020.

[111] Faraz Najafi, Jacob Mower, Nicholas C. Harris, Francesco Bellei, Andrew Dane, Catherine Lee, Xiaolong Hu, Prashanta Kharel, Francesco Marsili, Solomon Assefa, and et al. On-chip detection of non-classical light by scalable integration of single-photon detectors. *Nature Communications*, 6:5873, Jan 2015.

[112] Kae Nemoto, Michael Trupke, Simon J. Devitt, Ashley M. Stephens, Burkhard Scharfenberger, Kathrin Buczak, Tobias Nöbauer, Mark S. Everitt, Jörg Schmiedmayer, and William J. Munro. Photonic architecture for scalable quantum information processing in diamond. *Physical Review X*, 4:031022, Aug 2014.

[113] Michael A. Nielsen. Optical quantum computation using cluster states. *Physical Review Letters*, 93:040503, Jul 2004.

[114] J. R. Ong, R. Kumar, and S. Mookherjea. Ultra-high-contrast and tunable-bandwidth filter using cascaded high-order silicon microring filters. *IEEE Photonics Technology Letters*, 25(16):1543–1546, 2013.

[115] A. Osada, Y. Ota, R. Katsumi, M. Kakuda, S. Iwamoto, and Y. Arakawa. Strongly Coupled Single-Quantum-Dot–Cavity System Integrated on a CMOS-Processed Silicon Photonic Chip. *Physical Review Applied*, 11(2):024071, February 2019.

[116] Ardavan F. Oskooi, David Roundy, Mihai Ibanescu, Peter Bermel, J. D. Joannopoulos, and Steven G. Johnson. Meep: A flexible free-software package for electromagnetic simulations by the FDTD method. *Computer Physics Communications*, 181(3):687–702, March 2010.

[117] Stefano Paesani, Yunhong Ding, Raffaele Santagati, Levon Chakhmakhchyan, Caterina Vigliar, Karsten Rottwitt, Leif K. Oxenløwe, Jianwei Wang, Mark G. Thompson, and Anthony Laing. Generation and sampling of quantum states of light in a silicon chip. *Nature Physics*, 15(9):925–929, Sep 2019.

[118] Raj B. Patel, Anthony J. Bennett, Ian Farrer, Christine A. Nicoll, David A. Ritchie, and Andrew J. Shields. Two-photon interference of the emission from electrically tunable remote quantum dots. *Nature Photonics*, 4(9):632–635, Sep 2010.

[119] C. Pernice, W.and Schuck and O. et al. Minaeva. high-efficiency travelling wave single-photon detectors embedded in nanophotonic circuits. *Nature Communication*, 3(7948):1325, 2012.

[120] W. H. P. Pernice, C. Schuck, O. Minaeva, M. Li, G. N. Goltsman, A. V. Sergienko, and H. X. Tang. High-speed and high-efficiency travelling wave single-photon detectors embedded in nanophotonic circuits. *Nature Communications*, 3(1):1325, Dec 2012.

[121] Thomas Pertsch, Ulf Peschel, Falk Lederer, Jonas Burghoff, Matthias Will, Stefan Nolte, and Andreas Tünnermann. Discrete diffraction in two-dimensional arrays of coupled waveguides in silica. *Optics Letters.*, 29(5):468–470, Mar 2004.

[122] Alberto Peruzzo, Anthony Laing, Alberto Politi, Terry Rudolph, and Jeremy L. O'Brien. Multimode quantum interference of photons in multiport integrated devices. *Nature Communications*, 2(1):224, Mar 2011.

[123] Alberto Peruzzo, Jarrod McClean, Peter Shadbolt, Man-Hong Yung, Xiao-Qi Zhou, Peter J. Love, Alán Aspuru-Guzik, and Jeremy L. O'Brien. A variational eigenvalue solver on a photonic quantum processor. *Nature Communications*, 5(1):4213, Jul 2014.

[124] Frédéric Peyskens, Chitraleema Chakraborty, Muhammad Muneeb, Dries Van Thourhout, and Dirk Englund. Integration of single photon emitters in 2D layered materials with a silicon nitride photonic chip. *Nature Communications*, 10(1):4435, September 2019.

[125] Mateusz Piekarek, Damien Bonneau, Shigehito Miki, Taro Yamashita, Mikio Fujiwara,

Masahide Sasaki, Hirotaka Terai, Michael G. Tanner, Chandra M. Natarajan, Robert H. Hadfield, Jeremy L. O'Brien, and Mark G. Thompson. High-extinction ratio integrated photonic filters for silicon quantum photonics. *Optics Letters.*, 42(4):815–818, Feb 2017.

[126] J. Piprek. *Handbook of Optoelectronic Device Modeling and Simulation*, volume 2. CRC Press, Boca Raton, 2018.

[127] A. Politi, J. C. F. Matthews, M. G. Thompson, and J. L. O'Brien. Integrated quantum photonics. *IEEE Journal of Selected Topics in Quantum Electronics*, 15(6):1673–1684, 2009.

[128] Alberto Politi, Martin J. Cryan, John G. Rarity, Siyuan Yu, and Jeremy L. O'Brien. Silica-on-silicon waveguide quantum circuits. *Science*, 320(5876):646–649, 2008.

[129] Alberto Politi, Jonathan C. F. Matthews, and Jeremy L. O'Brien. Shor's quantum factoring algorithm on a photonic chip. *Science*, 325(5945):1221–1221, 2009.

[130] N. Prtljaga, R. J. Coles, J. O'Hara, B. Royall, E. Clarke, A. M. Fox, and M. S. Skolnick. Monolithic integration of a quantum emitter with a compact on-chip beam-splitter. *Applied Physics Letters*, 104(23):231107, 2014.

[131] Xiaogang Qiang, Xiaoqi Zhou, Jianwei Wang, Callum M. Wilkes, Thomas Loke, Sean O'Gara, Laurent Kling, Graham D. Marshall, Raffaele Santagati, Timothy C. Ralph, Jingbo B. Wang, Jeremy L. O'Brien, Mark G. Thompson, and Jonathan C. F. Matthews. Large-scale silicon quantum photonics implementing arbitrary two-qubit processing. *Nature Photonics*, 12(9):534–539, Sep 2018.

[132] Matthew T. Rakher and Kartik Srinivasan. Subnanosecond electro-optic modulation of triggered single photons from a quantum dot. *Applied Physics Letters*, 98(21):211103, May 2011.

[133] V. S. C. Manga Rao and S. Hughes. Single quantum dot spontaneous emission in a finite-size photonic crystal waveguide: Proposal for an efficient "on chip" single photon gun. *Physical Review Letters*, 99:193901, Nov 2007.

[134] Patrik Rath, Oliver Kahl, Simone Ferrari, Fabian Sproll, Georgia Lewes-Malandrakis, Dietmar Brink, Konstantin Ilin, Michael Siegel, Christoph Nebel, and Wolfram Pernice. Superconducting single-photon detectors integrated with diamond nanophotonic circuits. *Light: Science & Applications*, 4(10):e338–e338, Oct 2015.

[135] Patrik Rath, Sandeep Ummethala, Christoph Nebel, and Wolfram H. P. Pernice. Diamond as a material for monolithically integrated optical and optomechanical devices. *physica status solidi (a)*, 212(11):2385–2399, 2015.

[136] Robert Raussendorf and Hans J. Briegel. A one-way quantum computer. *Physical Review Letters*, 86:5188–5191, May 2001.

[137] G. Reithmaier, M. Kaniber, F. Flassig, S. Lichtmannecker, K. Müller, A. Andrejew, J. Vučković, R. Gross, and J. J. Finley. On-chip generation, routing, and detection of resonance fluorescence. *Nano Letters*, 15(8):5208–5213, 2015. PMID: 26102603.

[138] G. Reithmaier, M. Kaniber, F. Flassig, S. Lichtmannecker, K. Müller, A. Andrejew, J. Vučković, R. Gross, and J. J. Finley. On-Chip Generation, Routing, and Detection of Resonance Fluorescence. *Nano Lett.*, 15(8):5208–5213, August 2015.

[139] G. Reithmaier, S. Lichtmannecker, T. Reichert, P. Hasch, K. Muller, M. Bichler, R. Gross, and J. J. Finley. On-chip time resolved detection of quantum dot emission using integrated superconducting single photon detectors. *Sci. Rep.*, 3, May 2013.

[140] U. Rengstl, M. Schwartz, T. Herzog, F. Hargart, M. Paul, S. L. Portalupi, M. Jetter, and P. Michler. On-chip beamsplitter operation on single photons from quasi-resonantly excited quantum dots embedded in gaas rib waveguides. *Applied Physics Letters*, 107(2):021101, 2015.

[141] Lucio Robledo, Lilian Childress, Hannes Bernien, Bas Hensen, Paul F. A. Alkemade, and Ronald Hanson. High-fidelity projective read-out of a solid-state spin quantum register. *Nature*, 477(7366):574–578, Sep 2011.

[142] Sven Rodt, Stephan Reitzenstein, and Tobias Heindel. Deterministically fabricated solid-state quantum-light sources. *Journal of Physics: Condensed Matter*, 32(15):153003, 2020.

[143] Brendon C. Rose, Ding Huang, Zi-Huai Zhang, Paul Stevenson, Alexei M. Tyryshkin, Sorawis Sangtawesin, Srikanth Srinivasan, Lorne Loudin, Matthew L. Markham, Andrew M. Edmonds, Daniel J. Twitchen, Stephen A. Lyon, and Nathalie P. de Leon. Observation of an environmentally insensitive solid-state spin defect in diamond. *Science*, 361(6397):60–63, 2018.

[144] D. Sahin, A. Gaggero, Z. Zhou, S. Jahanmirinejad, F. Mattioli, R. Leoni, J. Beetz, M. Lermer, M. Kamp, S. Höfling, and et al. Waveguide photon-number-resolving detectors for quantum photonic integrated circuits. *Applied Physics Letters*, 103(11):111116, 2013.

[145] Döndü Sahin, Alessandro Gaggero, Thang Ba Hoang, Giulia Frucci, Francesco Mattioli, Roberto Leoni, Johannes Beetz, Matthias Lermer, Martin Kamp, Sven Höfling, and Andrea Fiore. Integrated autocorrelator based on superconducting nanowires. *Optics Express*, 21(9):11162–11170, May 2013.

[146] H. Sakata and S. Takeuchi. Grating-assisted directional coupler filters using algaas/gaas mqw waveguides. *IEEE Photonics Technology Letters*, 3(10):899–901, 1991.

[147] R Santagati, J W Silverstone, M J Strain, M Sorel, S Miki, T Yamashita, M Fujiwara, M Sasaki, H Terai, M G Tanner, C M Natarajan, R H Hadfield, J L O'Brien, and M G Thompson. Silicon photonic processor of two-qubit entangling quantum logic. *Journal of Optics*, 19(11):114006, oct 2017.

[148] Luca Sapienza, Marcelo Davanço, Antonio Badolato, and Kartik Srinivasan. Nanoscale optical positioning of single quantum dots for bright and pure single-photon emission. *Nature Communications*, 6(1):7833, Jul 2015.

[149] Alexander Schlehahn, Sarah Fischbach, Ronny Schmidt, Arsenty Kaganskiy, André Strittmatter, Sven Rodt, Tobias Heindel, and Stephan Reitzenstein. A stand-alone fiber-coupled single-photon source. *Scientific reports*, 8(1):1–7, 2018.

[150] Alexander Schlehahn, M Gaafar, M Vaupel, Manuel Gschrey, Peter Schnauber, J-H Schulze, Sven Rodt, André Strittmatter, W Stolz, A Rahimi-Iman, et al. Single-photon emission at a rate of 143 mhz from a deterministic quantum-dot microlens triggered by a mode-locked vertical-external-cavity surface-emitting laser. *Applied Physics Letters*, 107(4):041105, 2015.

[151] Alexander Schlehahn, Ronny Schmidt, C Hopfmann, J-H Schulze, André Strittmatter, Tobias Heindel, Liron Gantz, Emma R Schmidgall, David Gershoni, and Stephan Reitzenstein. Generating single photons at gigahertz modulation-speed using electrically controlled quantum dot microlenses. *Applied Physics Letters*, 108(2):021104, 2016.

[152] Peter Schnauber, Johannes Schall, Samir Bounouar, Theresa Höhne, Suk-In Park, Geun-Hwan Ryu, Tobias Heindel, Sven Burger, Jin-Dong Song, Sven Rodt, and Stephan Reitzenstein. Deterministic integration of quantum dots into on-chip multimode interference beamsplitters using in situ electron beam lithography. *Nano Letters*, 18(4):2336–2342, April 2018.

[153] Peter Schnauber, Johannes Schall, Samir Bounouar, Theresa Höhne, Suk-In Park, Geun-Hwan Ryu, Tobias Heindel, Sven Burger, Jin-Dong Song, Sven Rodt, and Stephan Reitzenstein. Deterministic integration of quantum dots into on-chip multimode interference beamsplitters using in situ electron beam lithography. *Nano Letters*, 18(4):2336–2342, 2018.

[154] Peter Schnauber, Ronny Schmidt, Arsenty Kaganskiy, Tobias Heuser, Manuel Gschrey, Sven Rodt, and Stephan Reitzenstein. Using low-contrast negative-tone pmma at cryogenic temperatures for 3d electron beam lithography. *Nanotechnology*, 27(19):195301, 2016.

[155] Peter Schnauber, Anshuman Singh, Johannes Schall, Suk In Park, Jin Dong Song, Sven Rodt, Kartik Srinivasan, Stephan Reitzenstein, and Marcelo Davanco. Indistinguishable photons from deterministically integrated single quantum dots in heterogeneous gaas/si3n4 quantum photonic circuits. *Nano Letters*, 19(10):7164–7172, 2019.

[156] Peter Schnauber, Anshuman Singh, Johannes Schall, Suk In Park, Jin Dong Song, Sven Rodt, Kartik Srinivasan, Stephan Reitzenstein, and Marcelo Davanco. Indistinguishable Photons from Deterministically Integrated Single Quantum Dots in Heterogeneous GaAs/Si3N4 Quantum Photonic Circuits. *Nano Letters*, 19(10):7164–7172, October 2019.

[157] Philipp-Immanuel Schneider, Nicole Srocka, Sven Rodt, Lin Zschiedrich, Stephan Reitzenstein, and Sven Burger. Numerical optimization of the extraction efficiency of a quantum-dot based single-photon emitter into a single-mode fiber. *Optics express*, 26(7):8479–8492, 2018.

[158] C. Schuck, X. Guo, L. Fan, X. Ma, M. Poot, and H. X. Tang. Quantum interference in heterogeneous superconducting-photonic circuits on a silicon chip. *Nature Communications*, 7(1):10352, January 2016.

[159] Andre Schwagmann, Sokratis Kalliakos, Ian Farrer, Jonathan P. Griffiths, Geb A. C. Jones, David A. Ritchie, and Andrew J. Shields. On-chip single photon emission from an integrated semiconductor quantum dot into a photonic crystal waveguide. *Applied Physics Letters*, 99(26):261108, 2011.

[160] Mario Schwartz, Ulrich Rengstl, Thomas Herzog, Matthias Paul, Jan Kettler, Simone Luca Portalupi, Michael Jetter, and Peter Michler. Generation, guiding and splitting of triggered single photons from a resonantly excited quantum dot in a photonic circuit. *Optics Express*, 24(3):3089–3094, Feb 2016.

[161] Mario Schwartz, Ekkehart Schmidt, Ulrich Rengstl, Florian Hornung, Stefan Hepp, Simone L. Portalupi, Konstantin llin, Michael Jetter, Michael Siegel, and Peter Michler. Fully on-chip single-photon hanbury-brown and twiss experiment on a monolithic semiconductor–superconductor platform. *Nano Letters*, 18(11):6892–6897, 2018.

[162] Lucas Schweickert, Klaus D. Jöns, Katharina D. Zeuner, Saimon Filipe Covre da Silva, Huiying Huang, Thomas Lettner, Marcus Reindl, Julien Zichi, Rinaldo Trotta, Armando Rastelli, and Val Zwiller. On-demand generation of background-free single photons from a solid-state source. *Applied Physics Letters*, 112(9):093106, 2018.

[163] Tae Joon Seok, Kyungmok Kwon, Johannes Henriksson, Jianheng Luo, and Ming C. Wu. 240×240 wafer-scale silicon photonic switches. In *Optical Fiber Communication Conference (OFC) 2019*, page Th1E.5. Optical Society of America, 2019.

[164] P. Shadbolt, M. Verde, and A. et al.. Peruzzo. Generating, manipulating and measuring entanglement and mixture with a reconfigurable photonic circuit. *Nature Photonics*, 6:45–49, 2012.

[165] J. Silverstone, Bonneau Santagati, R., and D. et al. Qubit entanglement between ring-resonator photon-pair sources on a silicon chip. *Nature Communication*, 6(7948):7948, 2015.

[166] J. W. Silverstone, D. Bonneau, J. L. O'Brien, and M. G. Thompson. Silicon quantum photonics. *IEEE Journal of Selected Topics in Quantum Electronics*, 22(6):390–402, 2016.

[167] Anshuman Singh, Qing Li, Shunfa Liu, Ying Yu, Xiyuan Lu, Christian Schneider, Sven Höfling, John Lawall, Varun Verma, Richard Mirin, Sae Woo Nam, Jin Liu, and Kartik Srinivasan. Quantum frequency conversion of a quantum dot single-photon source on a nanophotonic chip. *Optica*, 6(5):563–569, May 2019.

[168] Immo et al. sollner. Deterministic photon–emitter coupling in chiral photonic circuits. *Nature Nanotechnology*, 10(9):775, 2015.

[169] N. Somaschi, V. Giesz, L. De Santis, J. C. Loredo, M. P. Almeida, G. Hornecker, S. L. Portalupi, T. Grange, C. Antón, J. Demory, C. Gómez, I. Sagnes, N. D. Lanzillotti-Kimura,

A. Lemaître, A. Auffeves, A. G. White, L. Lanco, and P. Senellart. Near-optimal single-photon sources in the solid state. *Nature Photonics*, 10(5):340–345, May 2016.

[170] Belén Sotillo, Vibhav Bharadwaj, J. P. Hadden, Masaaki Sakakura, Andrea Chiappini, Toney Teddy Fernandez, Stefano Longhi, Ottavia Jedrkiewicz, Yasuhiko Shimotsuma, Luigino Criante, Roberto Osellame, Gianluca Galzerano, Maurizio Ferrari, Kiyotaka Miura, Roberta Ramponi, Paul E. Barclay, and Shane Michael Eaton. Diamond photonics platform enabled by femtosecond laser writing. *Scientific Reports*, 6(1):35566, Oct 2016.

[171] Chris Sparrow, Enrique Martín-López, Nicola Maraviglia, Alex Neville, Christopher Harrold, Jacques Carolan, Yogesh N. Joglekar, Toshikazu Hashimoto, Nobuyuki Matsuda, Jeremy L. O'Brien, David P. Tew, and Anthony Laing. Simulating the vibrational quantum dynamics of molecules using photonics. *Nature*, 557(7707):660–667, May 2018.

[172] J. P. Sprengers, A. Gaggero, D. Sahin, S. Jahanmirinejad, G. Frucci, F. Mattioli, R. Leoni, J. Beetz, M. Lermer, M. Kamp, and et al. Waveguide superconducting single-photon detectors for integrated quantum photonic circuits. *Applied Physics Letters*, 99(18):181110, 2011.

[173] Justin B. Spring, Paolo L. Mennea, Benjamin J. Metcalf, Peter C. Humphreys, James C. Gates, Helen L. Rogers, Christoph Söller, Brian J. Smith, W. Steven Kolthammer, Peter G. R. Smith, and Ian A. Walmsley. Chip-based array of near-identical, pure, heralded single-photon sources. *Optica*, 4(1):90–96, Jan 2017.

[174] Justin B. Spring, Benjamin J. Metcalf, Peter C. Humphreys, W. Steven Kolthammer, Xian-Min Jin, Marco Barbieri, Animesh Datta, Nicholas Thomas-Peter, Nathan K. Langford, Dmytro Kundys, James C. Gates, Brian J. Smith, Peter G. R. Smith, and Ian A. Walmsley. Boson sampling on a photonic chip. *Science*, 339(6121):798–801, 2013.

[175] N. Srocka, P. Mrowiński, J. Große, M. von Helversen, T. Heindel, S. Rodt, and S. Reitzenstein. Deterministically fabricated quantum dot single-photon source emitting indistinguishable photons in the telecom o-band. *Applied Physics Letters*, 116(23):231104, 2020.

[176] Nicole Srocka, Anna Musiał, P-I Schneider, Paweł Mrowiński, Paweł Holewa, Sven Burger, David Quandt, André Strittmatter, Sven Rodt, Stephan Reitzenstein, et al. Enhanced photon-extraction efficiency from ingaas/gaas quantum dots in deterministic photonic structures at 1.3 μ m fabricated by in-situ electron-beam lithography. *AIP Advances*, 8(8):085205, 2018.

[177] Yoshimasa Sugimoto, Yu Tanaka, Naoki Ikeda, Yusui Nakamura, Kiyoshi Asakawa, and Kuon Inoue. Low propagation loss of 0.76 db/mm in gaas-based single-line-defect two-dimensional photonic crystal slab waveguides up to 1 cm in length. *Optics Express*, 12(6):1090–1096, Mar 2004.

[178] Shuo Sun, Hyochul Kim, Zhouchen Luo, Glenn S. Solomon, and Edo Waks. A single-photon switch and transistor enabled by a solid-state quantum memory. *Science*, 361(6397):57–60, 2018.

[179] Alexander Szameit and Stefan Nolte. Discrete optics in femtosecond-laser-written photonic structures. *Journal of Physics B: Atomic, Molecular and Optical Physics*, 43(16):163001, jul 2010.

[180] Caterina Taballione, Tom A. W. Wolterink, Jasleen Lugani, Andreas Eckstein, Bryn A. Bell, Robert Grootjans, Ilka Visscher, Dimitri Geskus, Chris G. H. Roeloffzen, Jelmer J. Renema, Ian A. Walmsley, Pepijn W. H. Pinkse, and Klaus-J. Boller. reconfigurable quantum photonic processor based on silicon nitride waveguides. *Optics Express*, 27(19):26842–26857, Sep 2019.

[181] Allen Taflove and Susan C Hagness. *Computational electrodynamics: the finite-difference time-domain method; 3rd ed.* Artech House antennas and propagation library. Artech House, Boston, MA, 2005.

[182] Max Tillmann, Borivoje Dakić, René Heilmann, Stefan Nolte, Alexander Szameit, and Philip

Walther. Experimental boson sampling. *Nature Photonics*, 7(7):540–544, Jul 2013.

[183] E. Togan, Y. Chu, and A. et al. Trifonov. Quantum entanglement between an optical photon and a solid-state spin qubit. *Nature*, 466:730–740, 2010.

[184] Sebastian Unsleber, Yu-Ming He, Stefan Gerhardt, Sebastian Maier, Chao-Yang Lu, Jian-Wei Pan, Niels Gregersen, Martin Kamp, Christian Schneider, and Sven Höfling. Highly indistinguishable on-demand resonance fluorescence photons from a deterministic quantum dot micropillar device with 74% extraction efficiency. *Optics Express*, 24(8):8539–8546, Apr 2016.

[185] Maarten Van den Nest, Akimasa Miyake, Wolfgang Dür, and Hans J. Briegel. Universal resources for measurement-based quantum computation. *Physical Review Letters*, 97:150504, Oct 2006.

[186] J. Vuckovic, O. Painter, Yong Xu, A. Yariv, and A. Scherer. Finite-difference time-domain calculation of the spontaneous emission coupling factor in optical microcavities. *IEEE Journal of Quantum Electronics*, 35(8):1168–1175, August 1999.

[187] Noel H. Wan, Tsung-Ju Lu, Kevin C. Chen, Michael P. Walsh, Matthew E. Trusheim, Lorenzo De Santis, Eric A. Bersin, Isaac B. Harris, Sara L. Mouradian, Ian R. Christen, Edward S. Bielejec, and Dirk Englund. Large-scale integration of near-indistinguishable artificial atoms in hybrid photonic circuits. *arXiv:1911.05265 [quant-ph]*, November 2019. arXiv: 1911.05265.

[188] Hui Wang, Yu He, Yu-Huai Li, Zu-En Su, Bo Li, He-Liang Huang, Xing Ding, Ming-Cheng Chen, Chang Liu, Jian Qin, Jin-Peng Li, Yu-Ming He, Christian Schneider, Martin Kamp, Cheng-Zhi Peng, Sven Höfling, Chao-Yang Lu, and Jian-Wei Pan. High-efficiency multiphoton boson sampling. *Nature Photonics*, 11(6):361–365, Jun 2017.

[189] Hui Wang, Wei Li, Xiao Jiang, Y.-M. He, Y.-H. Li, X. Ding, M.-C. Chen, J. Qin, C.-Z. Peng, C. Schneider, M. Kamp, W.-J. Zhang, H. Li, L.-X. You, Z. Wang, J. P. Dowling, S. Höfling, Chao-Yang Lu, and Jian-Wei Pan. Toward scalable boson sampling with photon loss. *Physical Review Letters*, 120:230502, Jun 2018.

[190] Hui Wang, Jian Qin, Xing Ding, Ming-Cheng Chen, Si Chen, Xiang You, Yu-Ming He, Xiao Jiang, L. You, Z. Wang, C. Schneider, Jelmer J. Renema, Sven Höfling, Chao-Yang Lu, and Jian-Wei Pan. Boson sampling with 20 input photons and a 60-mode interferometer in a 10^{14}-dimensional hilbert space. *Physical Review Letters*, 123:250503, Dec 2019.

[191] Jianwei Wang, Stefano Paesani, Yunhong Ding, Raffaele Santagati, Paul Skrzypczyk, Alexia Salavrakos, Jordi Tura, Remigiusz Augusiak, Laura Mančinska, Davide Bacco, Damien Bonneau, Joshua W. Silverstone, Qihuang Gong, Antonio Acín, Karsten Rottwitt, Leif K. Oxenløwe, Jeremy L. O'Brien, Anthony Laing, and Mark G. Thompson. Multidimensional quantum entanglement with large-scale integrated optics. *Science*, 360(6386):285–291, 2018.

[192] Jianwei Wang, Alberto Santamato, Pisu Jiang, Damien Bonneau, Erman Engin, Joshua W. Silverstone, Matthias Lermer, Johannes Beetz, Martin Kamp, Sven Höfling, Michael G. Tanner, Chandra M. Natarajan, Robert H. Hadfield, Sander N. Dorenbos, Val Zwiller, Jeremy L. O'Brien, and Mark G. Thompson. Gallium arsenide (gaas) quantum photonic waveguide circuits. *Optics Communications*, 327:49 – 55, 2014. Special Issue on Nonlinear Quantum Photonics.

[193] Jianwei Wang, Fabio Sciarrino, Anthony Laing, and Mark G. Thompson. Integrated photonic quantum technologies. *Nature Photonics*, 14(5):273–284, May 2020.

[194] Yu-Jia Wei, Yu-Ming He, Ming-Cheng Chen, Yi-Nan Hu, Yu He, Dian Wu, Christian Schneider, Martin Kamp, Sven Höfling, Chao-Yang Lu, and Jian-Wei Pan. Deterministic and robust generation of single photons from a single quantum dot with 99.5% indistinguishability using adiabatic rapid passage. *Nano Letters*, 14(11):6515–6519, 2014.

[195] S. Weimann, M. Kremer, Y. Plotnik, Y. Lumer, S. Nolte, K. G. Makris, M. Segev, M. C. Rechtsman, and A. Szameit. Topologically protected bound states in photonic parity–time-symmetric crystals. *Nature Materials*, 16(4):433–438, Apr 2017.

[196] Daniel White, Artur Branny, Robert J. Chapman, Raphaël Picard, Mauro Brotons-Gisbert, Andreas Boes, Alberto Peruzzo, Cristian Bonato, and Brian D. Gerardot. Atomically-thin quantum dots integrated with lithium niobate photonic chips [Invited]. *Optical Materials Express*, 9(2):441–448, February 2019.

[197] Chi Xiong, Wolfram H. P. Pernice, Xiankai Sun, Carsten Schuck, King Y. Fong, and Hong X. Tang. Aluminum nitride as a new material for chip-scale optomechanics and nonlinear optics. *New Journal of Physics*, 14(9):095014, September 2012.

[198] Chi Xiong, Wolfram H. P. Pernice, and Hong X. Tang. Low-Loss, Silicon Integrated, Aluminum Nitride Photonic Circuits and Their Use for Electro-Optic Signal Processing. *Nano Letters*, 12(7):3562–3568, July 2012.

[199] Zhiliang Yuan, Beata E. Kardynal, R. Mark Stevenson, Andrew J. Shields, Charlene J. Lobo, Ken Cooper, Neil S. Beattie, David A. Ritchie, and Michael Pepper. Electrically driven single-photon source. *Science*, 295(5552):102–105, 2002.

[200] Iman Esmaeil Zadeh, Ali W. Elshaari, Klaus D. Jöns, Andreas Fognini, Dan Dalacu, Philip J. Poole, Michael E. Reimer, and Val Zwiller. Deterministic integration of single photon sources in silicon based photonic circuits. *Nano Letters*, 16(4):2289–2294, 2016.

[201] Haibin Zhang, Shane M. Eaton, and Peter R. Herman. Low-loss type ii waveguide writing in fused silica with single picosecond laser pulses. *Optics Express*, 14(11):4826–4834, May 2006.

[202] Xiaoyan Zhou, Irina Kulkova, Toke Lund-Hansen, Sofie Lindskov Hansen, Peter Lodahl, and Leonardo Midolo. High-efficiency shallow-etched grating on gaas membranes for quantum photonic applications. *Applied Physics Letters*, 113(25):251103, 2018.

[203] Kinga Żołnacz, Anna Musiał, Nicole Srocka, Jan Große, Maximilian J Schlösinger, Philipp-Immanuel Schneider, Oleh Kravets, Monika Mikulicz, Jacek Olszewski, Krzysztof Poturaj, et al. Method for direct coupling of a semiconductor quantum dot to an optical fiber for single-photon source applications. *Optics Express*, 27(19):26772–26785, 2019.